Scattering from Arbitrary Metal Particles

Using Green's Function Surface Integral Equation Method

Rasmus Risborg
Physics, 2020

Master's Project

Department of Materials and Production
Aalborg University
http://www.mp.aau.dk

AALBORG UNIVERSITY
STUDENT REPORT

Title:
Scattering from Arbitrary Metal Particles

Subtitle:
Using Green's Function Surface Integral Equation Method

Project Period:
Spring Semester 2020

Author:
Rasmus Risborg

Supervisor:
Thomas M. Søndergaard

Copies: 1

Page Numbers: 46

Date of Completion:
June 3, 2020

Abstract:

The purpose of this report is to model the scattering due to plane waves hitting metal particles of arbitrary shape, i.e. no symmetry is required for the scatterer. The metal is assumed to act like a perfect electric conductor PEC. The Green's Surface Integral Equation Method GFSIEM is used for modeling, specifically the Magnetic Field Integral Equation MFIE is used. Both a simple model based on a faceted representation of the scatterer surface, referred to as the Facet Method (FM) and a more advanced Curvilinear Model (CM) that represents the surface exactly is developed in this report. These models are compared to the analytical case of a sphere, and this shows good correspondence especially for the CM, however the scatter must be discretized very finely for small wavelengths. The CM is also compared to a GFSIEM model that uses cylindrical symmetry in the case of a rod, both methods give similar results.
The report also delves into the modifications that must be made to Green's function if the scatter is near an interface of dielectrica, rather than situated in free space.

Resumé

Denne rapport handler om at modellere spredningen forårsaget af at en plan bølge rammer en metal partikel/spreder. Metallet antages at agerer som en perfekt elektrisk leder, og der er ikke nogle krav til udformningen af partiklen i forhold til symmetri. Modelleringen er baseret på Green's Function Surface Integral Equation Method GFSIEM, mere specifikt bliver Magnetic Field Integral Equation MFIE brugt til at finde strømmen på sprederen. Både en simpel model baseret på en facetteret repræsentation af partiklens overflade, kaldet Facet Method, og en mere advanceret Curvilinear Method CM, som repræsenterer overfladen eksakt, bliver udviklet i denne rapport. Disse modeller bliver sammenlignet med den analytiske løsning for en sfære, der er god korrespondance mellem modellen og den analytiske løsning, især for CM, dog skal sprederen dikretiseres meget fint for små bølgelængder. CM bliver også sammen lignet med en cylinder symmetrisk version of GFSIEM for en stang spreder, også her giver begge modeller lignende resultater. Denne rapport gennemgår også hvilke ændringer der skal laves til Green's Function hvis sprederen er nær en grænseovergang mellem to dielektrika i stedet for at være suspenderet i frit rum.

Contents

1 Introduction **1**

2 Theoretical Background **3**
2.1 Scattering Theory 3
2.2 Green's Function Integral Equation Method 7

3 Facet Method **11**
3.1 The Method 11
3.2 Comparison with a Sphere 14

4 Curvilinear Method **19**
4.1 Curvilinear Triangles 20
4.1.1 Triangle on a Sphere 20
4.1.2 Triangle on a Cylinder 22
4.2 Subdivision 23
4.3 Facet and Curvilinear Method Comparison 25
4.4 Calculations for a Rod 27

5 Scatterer Near a Planar Interface **29**
5.1 Green's Functions for a Planar Interface 30
5.2 Singularity 33
5.2.1 Two Distinct Points on the Interface 35
5.2.2 Coinciding Points Above the Interface 36
5.3 Integration of a Descending Oscillating Function 36

6 Conclusion **39**

Bibliography **41**

A Analytic Solution for a Sphere **43**
A.1 Scattering Cross Section 45

Chapter 1

Introduction

There are many different methods for computationally modeling scattering, but this report focuses on one in particular: the Green's Function Surface Integral Equation Method (GFSIEM). This method can be applied to nano-particles and visible light [5] as well as for macroscopic antennas and radio waves, it is also sometimes known as the method of moments [1].

The primary source for this rapport is [5], which applies the GFIEM to a wide variety of cases, including an arbitrarily shaped particle in free space, however there are some modifications that need to be made for the purposes of this report. The benefit of the GFSIEM is that only the scatterer surface needs to be discretized, rather than needing to discretize the local area around the scatterer as well. There is an equivalent Green's Function method where the volume of the scatterer is discretized instead, but this makes it much harder to represent a scatterer with a smooth surface. Having a non smooth metal scatterer gives problems with the boundary conditions as we will see in chapter 2, which is why only smooth scatteres are considered in this report. Thus the geometry of the scatterer is not wholly arbitrary even though the title of this report is *Scattering from Arbitrary Metal Particles*, rather *arbitrary* refers to not requiring any kind of symmetry, this obviously makes the model more generally applicable. The metal is assumed to act like a perfect electric conductor PEC, which is valid when the effect of resistivity is negligible compared to other effects, in this case the incident field does not penetrate into the scatterer at all. This is not a trivial assumption, it does limit what can be modeled accurately, but there is also a lot to be gained by this approximation in terms of simplicity and speed of calculation.

Here the GFSIEM is based on the Magnetic Field Integral Equation MFIE instead of the Electric Field Integral Equation EFIE, which is done in [5], the idea behind this shift is to avoid numerically integrating over singularities. It is the PEC assumption that allows the complete avoidance of numerically integrating over a singularity.

The scattering is of course not just a product of the properties of the scatterer but also the environment, first off the scatterer is assumed to be situated in a homogeneous lossless dielectric, and later the effects on the scattering by the introduction of a single interface between two dielectrica is explored.

The theoretical background is outlined in Chapter 2, and the equations behind the GFSIEM are shown including how to solve the scattering problem with the help of the MFIE. A simple model based on a faceted representation of the scatterer, called the Facet Method is developed in Chapter 3. A more advanced model with an exact representation of the scatterer surface is developed in Chapter 4. Chapter 5 shows how the model must be modified when the scatterer is in the presence of an interface. Finally Chapter 6 contains the conclusion.

Chapter 2

Theoretical Background

This report deals with modeling the scattering of electromagnetic waves when it hits a metal scatterer. Section 2.1 starts off with a brief outline of the theory behind scattering, this also serves as a way to introduce the terms and notation used for the rest of the report. No model can handle every case, so Section 2.1 also defines the limits for this project, for example only scatterers that are perfect electric conductors (PEC) are dealt with.

Green's Function Surface Integral Equation Method is used for modeling, this method is described in [5, chapter 9], although there are some key differences, in that the method can be simplified here since we assume that the scatterer is a PEC. Furthermore we will use a GFSIEM based on the magnetic field integral equation as opposed to the source, which is based on the electric field instead. Everything pertaining to the GFSIEM is handled in Section 2.2.

2.1 Scattering Theory

For a more in depth overview of scattering theory see [5, chapter 2], for a detailed view of Maxwell's equations and the derivation of the boundary conditions see [2, chapter 7].

The general scattering problem is sketched in Figure 2.1. As mentioned there are limits to the the material and geometry of the scatterer, but first we must look at the assumptions for the environment and the incident electric field. The surrounding medium is assumed to be homogeneous, isotropic, linear, and non-magnetic, i.e. the medium has the permeability of free space. Now the medium can be described completely by the refractive index $n_1(\omega)$, which is a scalar function and where ω is angular frequency. The medium should also be lossless otherwise there would be no far field, thus n_1 is assumed to be real. Then the relative dielectric constant is simply given by $\varepsilon_1(\omega) = n_1^2(\omega)$.

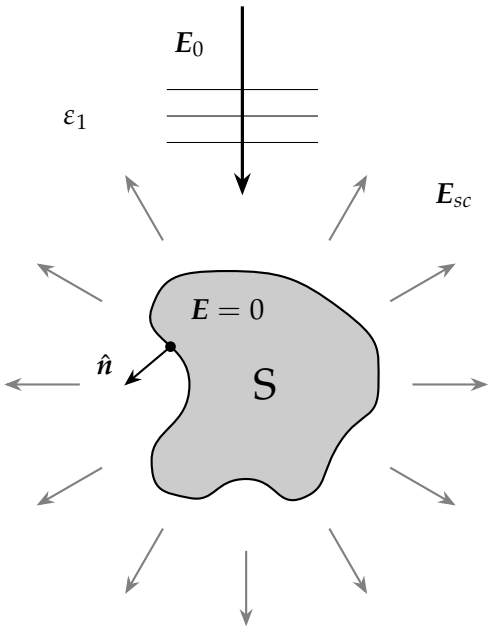

Figure 2.1: A plane wave $\boldsymbol{E}_0$ is incident on a scatterer situated in a medium with dielectric constant ε_1, which produces a scattered field $\boldsymbol{E}_{sc}$. The scatterer is a perfect electric conductor and therefore the electric field is zero inside the closed surface S, the normal vector $\hat{\boldsymbol{n}}$ always points away from the scatterer.

The incident light is assumed to be a plane wave, which can be written on the form

$$\boldsymbol{E}_0(\boldsymbol{r}) = \hat{\boldsymbol{p}} E_0 e^{i\boldsymbol{k}_1 \cdot \boldsymbol{r}}, \tag{2.1}$$

where $\boldsymbol{r}$ is a position, $\hat{\boldsymbol{p}}$ is the polarization vector, E_0 is the complex amplitude, $\boldsymbol{k}_1$ is the propagation vector outside the scatterer. The plane wave is time harmonic and (2.1) should be multiplied by $e^{-i\omega t}$, but this factor is suppressed throughout this report for convenience's sake. Omitting the time harmonic factor works particularly well because the scattered field $\boldsymbol{E}_{sc}$ has the same time dependence, and it simplifies Maxwell's equations greatly. The total electric field can be found as a simple sum, $\boldsymbol{E}(\boldsymbol{r}) = \boldsymbol{E}_0(\boldsymbol{r}) + \boldsymbol{E}_{sc}(\boldsymbol{r})$, keep in mind that this a complex field, the actual field is given by $\boldsymbol{E}_{(\text{actual})}(\boldsymbol{r}, t) = \text{Re}\{\boldsymbol{E}(\boldsymbol{r}) e^{-i\omega t}\}$. In the case of plane waves the magnetic field is given by $\boldsymbol{H} = \sqrt{\frac{\varepsilon_0}{\mu_0}} \hat{\boldsymbol{k}} \times \boldsymbol{E}$.

With these assumptions in mind Maxwell's equations can be written in terms of the electric field $\boldsymbol{E}$ and the magnetic field $\boldsymbol{H}$ as

$$\nabla \times \boldsymbol{E}(\boldsymbol{r}) = i\omega\mu_0 \boldsymbol{H}(\boldsymbol{r}), \tag{2.2a}$$

$$\nabla \times \boldsymbol{H}(\boldsymbol{r}) = \boldsymbol{j}(\boldsymbol{r}) - i\omega\varepsilon_0 \varepsilon \boldsymbol{E}(\boldsymbol{r}), \tag{2.2b}$$

$$\nabla \cdot \boldsymbol{E}(\boldsymbol{r}) = \frac{\rho}{\varepsilon_0 \varepsilon}, \tag{2.2c}$$

$$\nabla \cdot \boldsymbol{H}(\boldsymbol{r}) = 0, \tag{2.2d}$$

where ρ is the free charge density and $\boldsymbol{j}$ is the free current density. Then the wave equations can be found by using that $\nabla \times (\nabla \times A) = \nabla(\nabla \cdot A) - \nabla^2 A$:

$$-\nabla \times \nabla \times \boldsymbol{E}(\boldsymbol{r}) + k_0^2 \varepsilon_1 \boldsymbol{E}(\boldsymbol{r}) = -i\omega\mu_0 \boldsymbol{j}(\boldsymbol{r}) \tag{2.3}$$

$$-\nabla \times \nabla \times \boldsymbol{H}(\boldsymbol{r}) + k_0^2 \varepsilon_1 \boldsymbol{H}(\boldsymbol{r}) = -\nabla \times \boldsymbol{j}(\boldsymbol{r}), \tag{2.4}$$

where k_0 is the free space propagation number.

The perfect electric conductor is an idealized material with infinite conductivity, which makes it suited for modeling metals when the resistance is negligible compared to other effects. Working with a PEC carries many benefits when it comes to modeling scattering problems. Firstly there is no electric field inside the scatterer, nor a magnetic field, at least not a time harmonic field, consequently there is also no absorption. The properties of the PEC is unaffected by the frequency ω, if the environment is also frequency independent in the case of vacuum $n_1 = 1$, then the absolute size of the incoming wavelength and the scatterer does not matter, only the relative size.

If there are no sources $\rho = 0$ and $\boldsymbol{j} = 0$ then the wave equations for the surrounding environment reduces to

$$\left(\nabla^2 + k_0^2 \varepsilon_1\right) \boldsymbol{E}(\boldsymbol{r}) = 0, \qquad \nabla \cdot \boldsymbol{E}(\boldsymbol{r}) = 0, \tag{2.5}$$

$$\left(\nabla^2 + k_0^2 \varepsilon_1\right) \boldsymbol{H}(\boldsymbol{r}) = 0, \qquad \nabla \cdot \boldsymbol{H}(\boldsymbol{r}) = 0. \tag{2.6}$$

The boundary between the PEC and the medium must also be considered, in total there are four boundary conditions, for the normal and tangential part of both the magnetic and electric field:

$$\begin{aligned} \hat{\boldsymbol{n}} \times \boldsymbol{E}(\boldsymbol{r}) &= 0, & \hat{\boldsymbol{n}} \cdot \boldsymbol{E}(\boldsymbol{r}) &= \frac{\sigma(\boldsymbol{r})}{\varepsilon_0 \varepsilon}, \\ \hat{\boldsymbol{n}} \times \boldsymbol{H}(\boldsymbol{r}) &= \boldsymbol{J}(\boldsymbol{r}), & \hat{\boldsymbol{n}} \cdot \boldsymbol{H}(\boldsymbol{r}) &= 0, \end{aligned} \tag{2.7}$$

where $\boldsymbol{r}$ is a position on the surface, σ is the density of surface charge and $\boldsymbol{J}$ is the density of surface current. Physically what happens is that the incident field $\boldsymbol{E}_0$ hits the scatterer which generates the surface current $\boldsymbol{J}$ and surface charge density σ, such that the resulting field $\boldsymbol{E}_{sc}$ exactly cancels $\boldsymbol{E}_0$ everywhere inside the scatterer. Of course outside the scatter the fields generally do not cancel.

The scatterer must be a closed surface as this is required for the GFSIEM based on the magnetic equation [1, chapter 2]. The scatterer surface should also be smooth, as a jagged surface gives problems with the boundary conditions. For example if the surface has a 90° corner, then the normal vector will not be well defined in the corner, and the boundary conditions are therefore also not well defined. Choosing a smooth surface insures that the normal vector is uniquely defined at every point on the surface. However the scatterer does not need to adhere

to any symmetry rules and although *scatterer* is mentioned in the singular there could be multiple closed surfaces beside each other, as long as they do not intersect, for example the method could be used on a Yagi-Uda antenna.

the GFSIEM can find the scattered field anywhere given the surface current density $\boldsymbol{J}$ as we will see, $\boldsymbol{J}$ is usually simply referred to as the current hereafter. Thus knowing the current is the key to finding the scattered field and consequently answer questions such as how much light is scattered? and in what direction does it go?
The Poynting vector $\boldsymbol{S}$ describes the energy flux density of the fields, and it is given by

$$\boldsymbol{S} = \boldsymbol{E} \times \boldsymbol{H}. \tag{2.8}$$

This vector is time harmonic, however, we are interested in the time averaged Poynting vector

$$\langle \boldsymbol{S} \rangle = \frac{1}{T} \int_{t=0}^{T} \boldsymbol{S} dt = \frac{1}{2} \operatorname{Re}\{\boldsymbol{E} \times \boldsymbol{H}^*\}, \tag{2.9}$$

where $T = 2pi/\omega$ is the period. The intensity of the incident field is given by

$$I = \langle \boldsymbol{S}_0 \rangle = \frac{1}{2} \sqrt{\frac{\varepsilon_0}{\mu_0}} n |\boldsymbol{E}_0(\boldsymbol{r})|^2. \tag{2.10}$$

The total irradiated power of the scattered field P_{out} can be found by drawing a surface S_2 that encompasses the scatterer with a normal vector $\hat{\boldsymbol{n}}_2$ and then integrating the perpendicular part of the time averaged Poynting vector over this surface

$$P_{\text{out}} = \oint_{S_2} \langle \boldsymbol{S}(\boldsymbol{r}) \rangle \cdot \hat{\boldsymbol{n}}_2(\boldsymbol{r}) d^2 r. \tag{2.11}$$

In practice S_2 is a sphere that is much larger than the scatterer, a sphere is chosen because it is simple and a large sphere is chosen because then only a far field approximation of $\boldsymbol{E}_{sc}$ is needed. The scattered power can be normalized by the incident power per area to get the scattering cross section $\sigma_{sc} = P_{\text{out}}/I$ which has the units of area, despite the similar notation this has nothing to do with surface charges. Generally the scattering cross section is different from the actual cross sectional area, and is highly dependent on the incident wavelength, σ_{sc} can be much larger than the geometric cross section at resonances. Now assuming that S_2 is a sphere of radius r that envelops the scatterer then the scattering cross section is given by

$$\sigma_{sc} = \int_{\varphi=0}^{2\pi} \int_{\theta=0}^{\pi} \frac{1}{2} \sqrt{\frac{\varepsilon_0}{\mu_0}} n_1 |\boldsymbol{E}_{sc}(\boldsymbol{r})|^2 r^2 \sin\theta d\theta \, d\varphi. \tag{2.12}$$

there are also other optical cross sections, however the absorption cross section is zero because there is no absorption for a PEC, and the extinction cross section,

which is the amount of power lost from the incident beam is usually the sum of the scattering and absorption cross section, but here it is just equal to the scattering cross section.

So far we have looked at the total or integral scattering cross section σ_{sc}, but that is just a measure of the total energy loss it does not say anything about which direction the radiation has. This is motivation for introducing the differential scattering cross section $\frac{\partial \sigma_s c(\theta,\varphi)}{\partial \Omega}$, which is the cross section per solid angle, and it is equal to the integrand in (2.12) sans the $\sin\theta$ factor. For an example of what the total and differential scattering cross sections looks like see appendix A where the scattering from a sphere is calculated analytically.

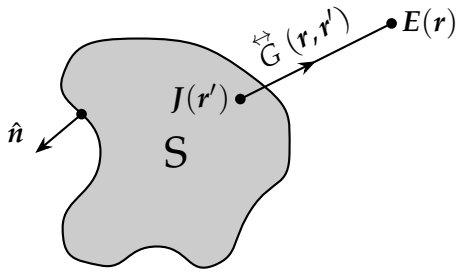

Figure 2.2: There is a contribution to the electric field $\boldsymbol{E}$ at point $\boldsymbol{r}$ from the current $\boldsymbol{J}$ at a point $\boldsymbol{r}'$ on the surface S. Green's tensor function $\overleftrightarrow{G}(\boldsymbol{r},\boldsymbol{r}')$ can determine this contribution.

2.2 Green's Function Integral Equation Method

As mentioned the GFSIEM can be based on the magnetic field and the electric field, the latter is the case in [5]. the EFIE is just as valid as the MFIE, however numerically there can be a big difference in how well it works. Since most of the work has already been done with the EFIE, these results are used unless there is a good reason to prefer the MFIE. It turns out that the MFIE is preferable when calculating the current, as this allows us to avoid numerically integrating over some singularities. So the GFSIEM used in this report is actually only partially based on the MFIE. Assume for now that the current $\boldsymbol{J}$ is known, then according to [5, Chapter 9] the electric field can be found anywhere outside the scatterer by

$$\boldsymbol{E}(\boldsymbol{r}) = \boldsymbol{E}_0(\boldsymbol{r}) + i\omega\mu_0 \oint_S \overleftrightarrow{G}(\boldsymbol{r},\boldsymbol{r}') \cdot \boldsymbol{J}(\boldsymbol{r}')d^2r', \tag{2.13}$$

where $\boldsymbol{r}'$ is a position on the surface S, this equation only hold because the scatterer is a PEC. The current at each point on the scatterer has an effect on the total field at any other location, and Green's tensor[1] function $\overleftrightarrow{G}(\boldsymbol{r},\boldsymbol{r}')$ describes the interaction as illustrated in Figure 2.2. Green's tensor does not change based on the shape of

[1]It is a tensor because the direction of the current and the resulting electric field matters.

the scatterer, it does however depend on the environment. Green's tensor is known for homogeneous space, for a detailed derivation see [3, Chapter 2], and it is given by

$$\overleftrightarrow{G}(\boldsymbol{r},\boldsymbol{r}') = \left(\overleftrightarrow{I} + \frac{1}{k_1^2}\nabla\nabla\right) g(\boldsymbol{r},\boldsymbol{r}'), \text{ where } g(\boldsymbol{r},\boldsymbol{r}') = \frac{e^{ik_1|\boldsymbol{r}-\boldsymbol{r}'|}}{4\pi|\boldsymbol{r}-\boldsymbol{r}'|} \tag{2.14}$$

$\overleftrightarrow{I} = \hat{\boldsymbol{x}}\hat{\boldsymbol{x}} + \hat{\boldsymbol{y}}\hat{\boldsymbol{y}} + \hat{\boldsymbol{z}}\hat{\boldsymbol{z}}$ is the unit dyadic, $g(\boldsymbol{r},\boldsymbol{r}')$ is called Green's scaler function. The gradients in this expression can be evaluated analytically and (2.14) can be written as

$$\overleftrightarrow{G}(\boldsymbol{r},\boldsymbol{r}') = \left(\overleftrightarrow{I}\left[1 + \frac{i}{k_1 R} - \frac{1}{(k_1 R)^2}\right] - \frac{\boldsymbol{R}\boldsymbol{R}}{R^2}\left[1 + \frac{3i}{k_1 R} - \frac{3}{(kR)^2}\right]\right) g(R), \tag{2.15}$$

where $\boldsymbol{R} = \boldsymbol{r} - \boldsymbol{r}'$ and $R = \|\boldsymbol{R}\|$.

To find the scattering cross section it is enough to know the far field expression for the scattered field, therefore it is beneficial to find a far field approximation of Green's tensor. Far away from the scatterer we have $r >> r'$ and $k_1 R >> 1$, where $r = \|\boldsymbol{r}\|$ and $r' = \|\boldsymbol{r}'\|$, then Green's tensor can be simplified to

$$\overleftrightarrow{G}(\boldsymbol{r},\boldsymbol{r}') \approx \left(\overleftrightarrow{I} - \frac{\boldsymbol{R}\boldsymbol{R}}{R^2}\right)\frac{e^{ikR}}{4\pi R}. \tag{2.16}$$

The distance R can be approximated as

$$R = r\sqrt{1 - 2\frac{\boldsymbol{r}\cdot\boldsymbol{r}'}{r} + \frac{\boldsymbol{r}'^2}{r^2}} \approx r - \hat{\boldsymbol{r}}\cdot\boldsymbol{r}'. \tag{2.17}$$

The distance R can be adequately approximated to be r in the denominators, but not in the exponent, as small differences can have a large effect on the phase. So $\frac{\boldsymbol{R}}{R} \approx \hat{\boldsymbol{r}}$ and $\overleftrightarrow{I} = \hat{\boldsymbol{r}}\hat{\boldsymbol{r}} + \hat{\boldsymbol{\theta}}\hat{\boldsymbol{\theta}} + \hat{\boldsymbol{\varphi}}\hat{\boldsymbol{\varphi}}$, therefore the far-field Green's tensor can be written as

$$\overleftrightarrow{G}^{(\mathrm{ff})}(\boldsymbol{r},\boldsymbol{r}') = \left(\hat{\boldsymbol{\theta}}\hat{\boldsymbol{\theta}} + \hat{\boldsymbol{\varphi}}\hat{\boldsymbol{\varphi}}\right)\frac{e^{ikr}}{4\pi r}e^{ik\hat{\boldsymbol{r}}\cdot\boldsymbol{r}'}. \tag{2.18}$$

Finally the scattered far-field can be found

$$E_{sc}^{(\mathrm{ff})}(\boldsymbol{r}) = i\omega\mu_0\left(\hat{\boldsymbol{\theta}}\hat{\boldsymbol{\theta}} + \hat{\boldsymbol{\varphi}}\hat{\boldsymbol{\varphi}}\right)\frac{e^{ikr}}{4\pi r}\oint_S e^{-ik\hat{\boldsymbol{r}}\cdot\boldsymbol{r}'}\boldsymbol{J}(\boldsymbol{r}')d^2r'. \tag{2.19}$$

Now we are ready to tackle the problem of finding the current $\boldsymbol{J}$. First we can find an magnetic field equivalent of (2.13) by using that $\nabla\times\boldsymbol{E}(\boldsymbol{r}) = i\omega\mu_0\boldsymbol{H}(\boldsymbol{r})$:

$$\boldsymbol{H}(\boldsymbol{r}) = \boldsymbol{H}_0(\boldsymbol{r}) + \oint_S \nabla\times\overleftrightarrow{G}(\boldsymbol{r},\boldsymbol{r}')\cdot\boldsymbol{J}(\boldsymbol{r}')d^2r', \tag{2.20}$$

where $H_0(\boldsymbol{r})$ is the incident magnetic field. When $\boldsymbol{r}$ approaches the surface we can find the current at this location by using the boundary condition $\boldsymbol{J}(\boldsymbol{r}) = \hat{\boldsymbol{n}}(\boldsymbol{r}) \times \boldsymbol{H}(\boldsymbol{r})$ to get

$$\boldsymbol{J}(\boldsymbol{r}) = \boldsymbol{J}_0(\boldsymbol{r}) + \oint_S \hat{\boldsymbol{n}} \times [\nabla \times \overleftrightarrow{G}(\boldsymbol{r}, \boldsymbol{r}')] \cdot \boldsymbol{J}(\boldsymbol{r}') d^2 r', \tag{2.21}$$

where $\boldsymbol{J}_0 = \hat{\boldsymbol{n}} \times \boldsymbol{H}_0$, note that $\hat{\boldsymbol{n}}$ is a function of $\boldsymbol{r}$ and not $\boldsymbol{r}'$. To find an expression for the integrand we can use that the curl of a gradient is zero and that $\overleftrightarrow{I} \cdot \boldsymbol{J}(\boldsymbol{r}') = \boldsymbol{J}(\boldsymbol{r}')$ to get

$$\hat{\boldsymbol{n}} \times \left[\nabla \times \overleftrightarrow{G}(\boldsymbol{r}, \boldsymbol{r}')\right] \cdot \boldsymbol{J}(\boldsymbol{r}') = \hat{\boldsymbol{n}} \times \left[\nabla \times \left[g(\boldsymbol{r}, \boldsymbol{r}') \boldsymbol{J}(\boldsymbol{r}')\right]\right] \tag{2.22}$$

Now the following identity can be used $\nabla \times (\psi \boldsymbol{A}) = \psi \nabla \times \boldsymbol{A} + (\nabla g(\boldsymbol{r}, \boldsymbol{r}')) \times \boldsymbol{A}$, and we know that $\nabla \times \boldsymbol{J}(\boldsymbol{r}') = 0$, because it does not depend on $\boldsymbol{r}$, to get

$$\hat{\boldsymbol{n}} \times \left[\nabla \times \overleftrightarrow{G}(\boldsymbol{r}, \boldsymbol{r}')\right] \cdot \boldsymbol{J}(\boldsymbol{r}') = \hat{\boldsymbol{n}} \times \left[\left(\nabla g(\boldsymbol{r}, \boldsymbol{r}')\right) \times \boldsymbol{J}(\boldsymbol{r}')\right]. \tag{2.23}$$

The gradient of the scalar Green's function can be found to be

$$\nabla g(\boldsymbol{r}, \boldsymbol{r}') = \frac{\boldsymbol{R}}{R} \left(ik_1 - \frac{1}{R}\right) g(\boldsymbol{r}, \boldsymbol{r}'). \tag{2.24}$$

Finally the integrand can be written as

$$\hat{\boldsymbol{n}} \times \left[\nabla \times \overleftrightarrow{G}(\boldsymbol{r}, \boldsymbol{r}')\right] \cdot \boldsymbol{J}(\boldsymbol{r}') = \left(ik_1 - \frac{1}{R}\right) g(\boldsymbol{r}, \boldsymbol{r}') \left[\frac{\boldsymbol{R}}{R} \left(\hat{\boldsymbol{n}}(\boldsymbol{r}) \cdot \boldsymbol{J}(\boldsymbol{r}')\right) - \boldsymbol{J}(\boldsymbol{r}') \left(\hat{\boldsymbol{n}}(\boldsymbol{r}) \cdot \frac{\boldsymbol{R}}{R}\right)\right], \tag{2.25}$$

where the identity: $\boldsymbol{A} \times \boldsymbol{B} \times \boldsymbol{C} = \boldsymbol{B}(\boldsymbol{A} \cdot \boldsymbol{C}) - \boldsymbol{C}(\boldsymbol{A} \cdot \boldsymbol{B})$ has been used.

As the position $\boldsymbol{r}$ approaches the sampling point $\boldsymbol{s}$ on the surface, there is a singularity when $\boldsymbol{r}' = \boldsymbol{s}$, which fortunately can be handled analytically. The integral can be split up into two parts, one integral over an infinitesimal circle around $\boldsymbol{s}$ and one principal integral over the rest of the surface. If we define the coordinate system such that the normal vector at $\boldsymbol{s}$ is along the z-axis, and if the surface is smooth and $\boldsymbol{r}'$ is sufficiently close to $\boldsymbol{s}$, then the surface is in the x, y-plane: $\boldsymbol{r}' = \boldsymbol{s} + \rho' \hat{\boldsymbol{\rho}}'$. The position $\boldsymbol{r}$ is set to be a small distance δ away from the surface $\boldsymbol{r} = \boldsymbol{s} + \delta \hat{\boldsymbol{n}}$. The dot-product $(\hat{\boldsymbol{n}} \cdot \boldsymbol{J}(\boldsymbol{r}'))$ will vanish as $\hat{\boldsymbol{n}}$ and $\boldsymbol{J}$ are orthogonal close to $\boldsymbol{s}$. The other dot-product on the other hand is non-zero and is given by $\hat{\boldsymbol{n}} \cdot \frac{\boldsymbol{R}}{R} = \frac{\delta}{\sqrt{\delta^2 + \rho'^2}}$. Then the singular part of the integral in (2.21) is

$$\int_0^{2\pi} \int_0^a \boldsymbol{J}(\boldsymbol{r}') \frac{e^{ik_1 R}}{4\pi} \left[\hat{\boldsymbol{n}} \cdot \frac{\boldsymbol{R}}{R^3}\right] \rho' d\rho' \, d\varphi' \approx \frac{\boldsymbol{J}(\boldsymbol{r})}{2} \int_0^a \frac{\delta \rho'}{\left(\delta^2 + a^2\right)^{3/2}} d\rho', \tag{2.26}$$

where it has been used that there is no φ-dependence, and that $\boldsymbol{J}(\boldsymbol{r}') \approx \boldsymbol{J}(\boldsymbol{r})$ and $e^{ik_1 R} \approx 1$ for $\boldsymbol{r}' \to \boldsymbol{r}$.

The integral is easy to solve using substitution and when $\delta \to 0$ the integral is found to be

$$\frac{\boldsymbol{J}(\boldsymbol{r})}{2} \int_0^a \frac{\delta\rho'}{(\delta^2 + a^2)^{3/2}} d\rho' \to \frac{\boldsymbol{J}(\boldsymbol{r})}{2} \quad \text{for} \quad \delta \to 0. \tag{2.27}$$

Then (2.21) can be written in terms of a principal integral as

$$\frac{\boldsymbol{J}(\boldsymbol{r})}{2} = \boldsymbol{J}_0(\boldsymbol{r}) + P \oint_S \hat{\boldsymbol{n}} \times [\nabla \times \overleftrightarrow{G}(\boldsymbol{r}, \boldsymbol{r}')] \cdot \boldsymbol{J}(\boldsymbol{r}') d^2 r'. \tag{2.28}$$

Now we have all we need to develop a GFSIEM model for scattering.

Chapter 3

Facet Method

To find the electric field at any location we need to know the current for every location on the scatterer, of course this is not generally possible so we must contend ourselves with finding the current on N points on the surface and then interpolate the current between the known points. There are many ways of achieving this, in this chapter we will look at a simple implementation of the GFSIEM, which we can call the Facet Method, and then see how well it fits with the known results of a sphere.

3.1 The Method

The Facet Method consists of dividing the surface into N triangles, giving it a faceted surface, hence the name, and then assume that the current is constant on each triangle and equal to the current in the center of the triangle. This is a rudimentary model that does not accurately represent the reality, because the scatterer should be smooth and the current should also be a smooth function. However, as the number of triangles go up, the surface and current are more accurately represented.

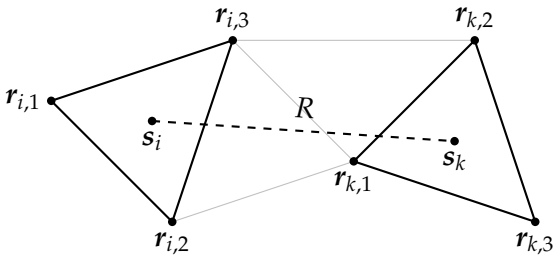

Figure 3.1: The whole surface of the scatterer is divided into triangles and they should be roughly equilateral. The GFSIEM requires finding the coupling between each pair of triangles, where they have a center-to-center distance of R. There is also self-coupling in the case where $i = k$.

The surface is divided into a total of N triangles, the k'th triangle has three corners given by $\boldsymbol{r}_{k,j}$, where $j = 1, 2, 3$, as illustrated in Figure 3.1. This task is accomplished by using the Partial Differential Equation Toolbox in MATLAB. All the relevant information can be stored in a point and a connectivity matrix.

The corner points for all the triangles are stored in a point matrix $\overline{\overline{\boldsymbol{P}}}$, so that each column contains a unique x, y and z coordinate for a corner point,

$$\overline{\overline{\boldsymbol{P}}} = \begin{bmatrix} x_1 & x_2 & \dots & x_M \\ y_1 & y_2 & \dots & y_M \\ z_1 & z_2 & \dots & z_M \end{bmatrix}, \tag{3.1}$$

note that each corner point is shared among several triangles.
The connectivity matrix $\overline{\overline{\boldsymbol{T}}}$ stores information about each triangle in a column, such that all the pertinent information about the k'th triangle is in the k'th column of $\overline{\overline{\boldsymbol{T}}}$. First and foremost the connectivity matrix $\overline{\overline{\boldsymbol{T}}}$ describes the three points that make up the vertices of each triangle. Thus the simplest form of $\overline{\overline{\boldsymbol{T}}}$ is a $3\times N$ matrix, where each element is an index for a column of the point matrix. The connectivity matrix can have any number of rows for holding additional information, for example the three components of the normal vector, in this case the connectivity matrix would be a $6\times N$-matrix. Thus the connectivity matrix will be on the form

$$\overline{\overline{\boldsymbol{T}}} = \left[\begin{array}{cccc} i_{1,1} & i_{2,1} & \dots & i_{N,1} \\ i_{1,2} & i_{2,2} & \dots & i_{N,2} \\ i_{1,3} & i_{2,3} & \dots & i_{N,3} \\ \hline \vdots & \vdots & \vdots & \vdots \end{array}\right], \tag{3.2}$$

where the j'th corner point of the k'th triangle, $\boldsymbol{r}_{k,j}$, is given by the $i_{k,j}$'th column of the point matrix $\overline{\overline{\boldsymbol{P}}}$.
In this simple method we are only interested in sampling the current at the center point of the triangles, and then we assume that the current is constant. The sampling points can easily be found by averaging: $\boldsymbol{s}_k = (\boldsymbol{r}_{k,1} + \boldsymbol{r}_{k,1} + \boldsymbol{r}_{k,3})/3$.

It is convenient to introduce an orthonormal basis for each triangle, where one the basis vectors is the normal vector, then the surface current will be a linear combination of the two other basis vectors. One of the benefits of the Facet Method is that the basis vectors are the same over each triangle, as the normal vector is constant. The basis vectors for each triangle can for example be defined as

$$\hat{\boldsymbol{t}}_k^{(1)} = \frac{\boldsymbol{r}_{k,2} - \boldsymbol{r}_{k,1}}{\|\boldsymbol{r}_{k,2} - \boldsymbol{r}_{k,1}\|} \tag{3.3}$$

$$\hat{\boldsymbol{t}}_k^{(2)} = \hat{\boldsymbol{n}}_k \times \hat{\boldsymbol{t}}_k^{(1)}, \tag{3.4}$$

where $\hat{\boldsymbol{n}}_k$ is the normal vector for the k'th triangle and a basis vector as mentioned. Now the surface current at $\boldsymbol{s}_k$ can be written as

$$\boldsymbol{J}_k = J_k^{(1)} \hat{\boldsymbol{t}}_k^{(1)} + J_k^{(2)} \hat{\boldsymbol{t}}_k^{(2)}. \tag{3.5}$$

A similar definition can be applied to $\boldsymbol{J}_0$ and then (2.28) can be written as

$$J_{0,i}^{(1)}\hat{\boldsymbol{t}}_i^{(1)} + J_{0,i}^{(2)}\hat{\boldsymbol{t}}_i^{(2)} =$$
$$\frac{1}{2}\left(J_i^{(1)}\hat{\boldsymbol{t}}_i^{(1)} + J_i^{(2)}\hat{\boldsymbol{t}}_i^{(2)}\right) - \sum_{k=1}^{N} P\int_k \hat{\boldsymbol{n}}\times\left[\nabla\times\overleftrightarrow{G}\left(\boldsymbol{s_i},\boldsymbol{r}'\right)\right]\cdot\left(J_k^{(1)}\hat{\boldsymbol{t}}_k^{(1)} + J_k^{(2)}\hat{\boldsymbol{t}}_k^{(2)}\right)dr'^2, \quad (3.6)$$

where the integral is over the area of the k'th triangle and $\hat{\boldsymbol{n}}$ is the normal vector for triangle i. This needs to repeated for $i = 1$ to N, which can be written as this matrix equation:

$$\begin{bmatrix}\overline{J}_0^{(1)}\\ \overline{J}_0^{(2)}\end{bmatrix} = -\begin{bmatrix}\left(\overline{\overline{\boldsymbol{K}}}^{(1,1)} - \frac{1}{2}\overline{\overline{\boldsymbol{I}}}\right) & \overline{\overline{\boldsymbol{K}}}^{(1,2)}\\ \overline{\overline{\boldsymbol{K}}}^{(2,1)} & \left(\overline{\overline{\boldsymbol{K}}}^{(2,2)} - \frac{1}{2}\overline{\overline{\boldsymbol{I}}}\right)\end{bmatrix}\begin{bmatrix}\overline{J}^{(1)}\\ \overline{J}^{(2)}\end{bmatrix}, \quad (3.7)$$

where the currents are arranged in column vectors where the k'th element is the corresponding current in the k'th triangle $\overline{J}^{(m)} = [J_1^{(m)}\ J_2^{(m)}\ \dots\ J_N^{(m)}]^T$.

The $\overline{\overline{\boldsymbol{K}}}$ matrices are on the form

$$\overline{\overline{\boldsymbol{K}}}^{(m,n)} = \begin{bmatrix}K_{11}^{(m,n)} & K_{12}^{(m,n)} & \cdots & K_{1N}^{(m,n)}\\ K_{21}^{(m,n)} & K_{22}^{(m,n)} & \cdots & K_{2N}^{(m,n)}\\ \vdots & \vdots & \ddots & \vdots\\ K_{N1}^{(m,n)} & K_{N2}^{(m,n)} & \cdots & K_{NN}^{(m,n)}\end{bmatrix}, \quad (3.8)$$

where the elements are defined as

$$K_{ik}^{(m,n)} = P\int_k \hat{\boldsymbol{t}}_i^{(m)}\cdot\left[\hat{\boldsymbol{n}}\times\left[\nabla\times\overleftrightarrow{G}\left(\boldsymbol{s}_i,\boldsymbol{r}'\right)\right]\right]\cdot\hat{\boldsymbol{t}}_k^{(n)}dr'^2. \quad (3.9)$$

The self-term principal integrals, i.e. when $i = k$, can be solved analytically, as the normal vector $\hat{\boldsymbol{n}}_i$ is orthogonal to $\boldsymbol{J}_i$ and $\boldsymbol{R}/R$ on the whole triangle, except just around the singularity. Thus it is easy to see that the integrand (2.25) is zero everywhere in the principal integral, and the integral evaluates to zero. Therefore the diagonal of the $\overline{\overline{\boldsymbol{K}}}$'s are empty.

The integral in (3.9) can be approximated by only evaluating Green's tensor in the center point, $\boldsymbol{r}' = \boldsymbol{s}_k$, and then multiplying by the area of the triangle A_k:

$$K_{ik}^{(m,n)} \approx \hat{\boldsymbol{t}}_i^{(m)}\cdot\left[\hat{\boldsymbol{n}}\times\left[\nabla\times\overleftrightarrow{G}\left(\boldsymbol{s}_i,\boldsymbol{s}_k\right)\right]\right]\cdot\hat{\boldsymbol{t}}_k^{(n)}A_k, \quad (3.10)$$

we can call this the centroidal approximation. This approximation makes the simulation much faster, and in the next section we will see how well this rather simple method works compared to a known case.

3.2 Comparison with a Sphere

The sphere is a case where the scattering can be found analytically, which makes it possible to compare the Facet Method to a known result. The analytical expressions for the surface current and the scattering cross section can be found in appendix A.

First we will look at the surface conductivity, and the difference compared to the analytical result at a single wavelength. A wavelength equal to the diameter of the sphere is chosen, because we are interested in seeing how well the model works when the wavelgnth is comparable to the size of the scatterer. Specifically the radius is $a = 10\,\text{nm}$ and the wavelength is $\lambda = 20\,\text{nm}$, the unit does not really matter as only the relative size matters. As rule of thumb the average side length of the triangles should be about a tenth or less of the wavelength, in our case choosing $N = 800$ makes this length 1.92 nm, so the rule is satisfied. Figure 3.2a shows the absolute value of the surface conductivity for the sphere calculated by the facet method, this is visually indistinguishable from the analytical result, thus it is helpful to look at the relative difference between the calculated and actual result. Figure 3.2b shows this difference, and it is calculated in the following way

$$J_{k,\text{diff}} = \frac{\|\boldsymbol{J}_{k,\text{ana}}\| - \|\boldsymbol{J}_{k,\text{num}}\|}{\max_{1\leq i\leq N} \|\boldsymbol{J}_{i,\text{ana}}\|} \cdot 100\%. \tag{3.11}$$

The difference between the numerical and analytical current is at most 5% often less, which is not bad for such a simple method. So we have seen that this method can model wavelengths comparable to the size of the scatterer without a huge N, it will be interesting to see how small the wavelengths can get before the results deviates too much from the actual result. Later we will see how accurate the numerically calculated currents are for a wide range of wavelengths, but first we will look at the scattering cross section.

The scattering cross section can also be found analytically and numerically on the basis of the surface currents found above. The cross section is plotted against the wavelength divided by the diameter ($\lambda/2a$) in Figure 3.3. It can be seen that the numerical method is unstable for low wavelengths, even lower than shown is too unstable to be useful. There is even some instability for the numerical result with $N = 800$ when the wavelength is around 1.1 times the diameter, even though the side length is comparatively small. Still the result is close to the actual, and more triangular divisions are better as expected. We can also see that for large wavelengths where the sidelength/wavelength ratio is small, the analytical cross section is larger than the numerical, this pattern is continued for even larger wavelengths than shown. The reason for this is that the faceted sphere is strictly smaller than the real sphere, which results in a smaller effective cross section compared

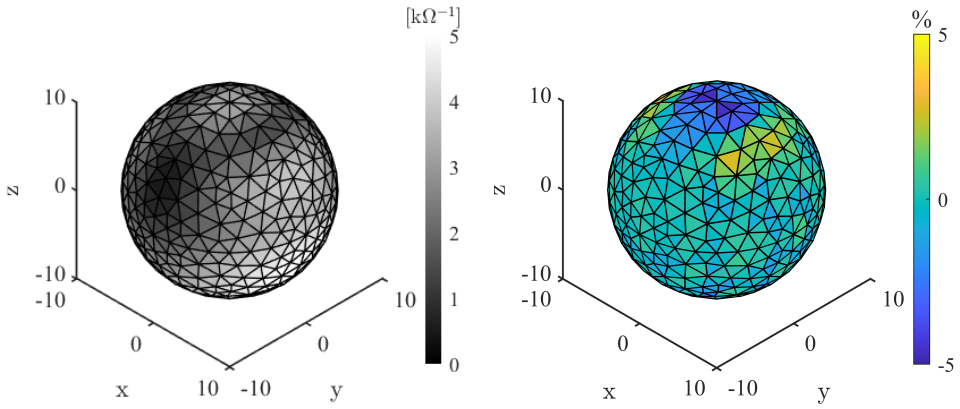

Figure 3.2: Calculations for the absolute value of the conduction for a sphere with radius 10 nm, and $N = 800$. The sphere is illuminated from below by a x-polarized plane wave with wavelength 20 nm. **(a)** Absolute surface conduction calculated with the numerical method. **(b)** Difference in percent between the analytical and numerical solution.

to the geometrical cross section, πa^2. The case with $N = 208$ is much worse than the case with $N = 800$ even for large wavelengths because it is smaller. Thus there are two important consideration to make when choosing N: are the sidelengths sufficiently small for the wavelengths and is the shape accurately represented.

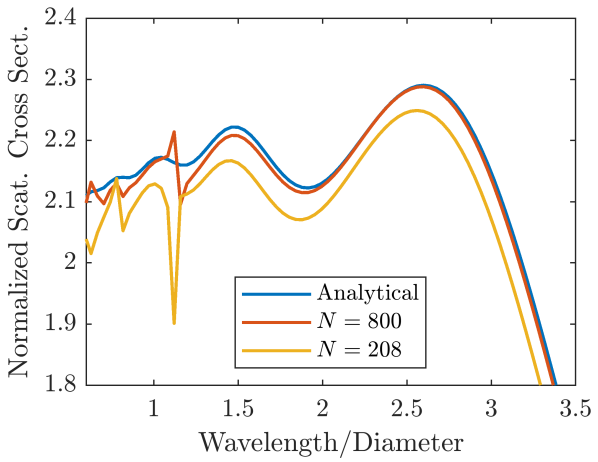

Figure 3.3: Scattering cross section for sphere illuminated from below with a range of wavelengths compared to the diameter. Both the analytical result and numerical result is shown, where a different number of triangles N is used.

Next an expression for the total error will be introduced and we will see graphs for the error against wavelength for different conditions. The error can be defined as

$$F = \frac{\sum_{k=1}^{N} \left| \|\boldsymbol{J}_{k,\text{ana}}\| - \|\boldsymbol{J}_{k,\text{num}}\| \right| A_k}{\sum_{k=1}^{N} \|\boldsymbol{J}_{k,\text{ana}}\| A_k}. \tag{3.12}$$

This is a measurement of the difference between the analytical and numerical current, instead the error could be defined based on the scattering cross section, but the trends should be the same.

The error F is plotted in Figure 3.4. For a sense of what the error means we can see that for the case shown in Figure 3.2 the corresponding error is slightly above 10^{-2}. The pattern we saw from the scattering cross section can also be seen here, but perhaps more clearly, especially the part where the error approaches some constant value due to the inaccurate representation of the scatterer geometry. A higher number N is evidently better as expected, and in the case where $N = 800$ the current is accurately calculated down to a wavelength that is equal to the radius.

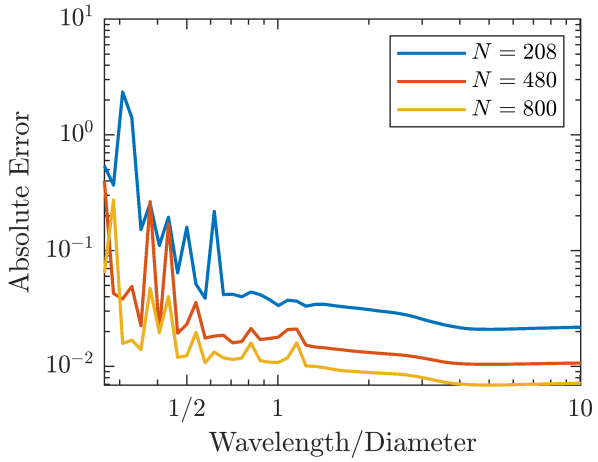

Figure 3.4: The Error F for the numerical model for various N on a logarithmic scale. The error is unstable and large for small wavelengths, the error levels off to be a roughly constant value for large wavelengths. The Error also becomes smaller as N increases.

As we can see the Facet Method does approach the analytical result to decent degree without requiring a huge number of triangles. The benefit of this method is that it can easily represent any closed shape. However, we can see that the inaccurate reproduction of the exact surface produces a floor for how well the method can work for large wavelengths.

There is likely something to be gained by representing the surface accurately, which is more challenging and effectively limits the complexity of the scatterer, this will be the subject of the next chapter. The time to calculate and more alarmingly the memory for calculating the surface currents goes up with N, the hope is with an accurate surface, then the required N and goes down for a given wavelength within a certain error. Still the Facet Method does well for how simple it is, it can even represent complex scatterers with ease.

Chapter 4

Curvilinear Method

In this chapter we will see how the Facet Method can be improved by representing the scatterer surface accurately. This is accomplished by dividing the scatterer into triangles as before, however, this time the triangles themselves are curvilinear, for an example of a spherical triangle see Figure 4.1. How the curvilinear triangles work in detail is considered in section 4.1, although this report is only concerned with curvilinear triangles that are either a part of a cylinder or a sphere. The centroidal approximation from the previous chapter is also something that can be developed upon, which is examined in section 4.2. Section 4.3 compares the Curvilinear Method (CM) to the Facet Method (FM).

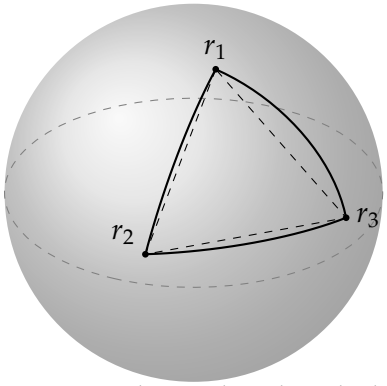

Figure 4.1: For three corner points $\boldsymbol{r}_1$, $\boldsymbol{r}_2$ and $\boldsymbol{r}_3$ on the sphere, both a flat and spherical triangle can be formed. The edges for the spherical triangle are along the shortest path on the sphere between the corner pairs. For the underlying flat triangle, marked with a dashed line, it is the euclidean shortest path that marks the edges.

4.1 Curvilinear Triangles

As mentioned in the previous chapter the complexity of representing any arbitrary shape goes up when the surface is to be exact instead of faceted, thus in this report the scatterer is limited to consist of sections that are either flat, cylindrical or spherical. Even with this restriction a large number of interesting geometries can be explored. Now the idea is to first produce the faceted surface as before and then project a point on the flat triangle, $\boldsymbol{r}_k$, out onto the exact surface, $\boldsymbol{r}_k^{(\text{exact})}$. First we need a way to represent a point on the flat triangle in a way that does not depend on the orientation of the triangle, this can be done by introducing a triangular coordinate system via the parameters u and v:

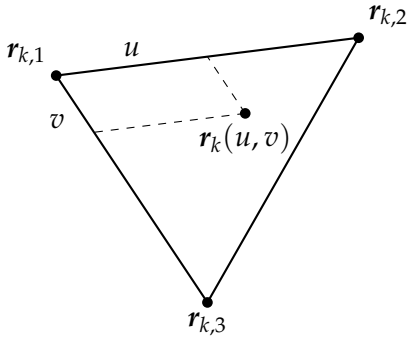

Figure 4.2: Illustration of triangular coordinates, in this case $u = 0.5$ and $v = 0.25$.

$$\boldsymbol{r}_k(u,v) = \boldsymbol{r}_{k,1} + u(\boldsymbol{r}_{k,2} - \boldsymbol{r}_{k,1}) + v(\boldsymbol{r}_{k,3} - \boldsymbol{r}_{k,1}), \tag{4.1}$$

where $0 \leq u + v \leq 1$ and $u, v \geq 0$ and it is illustrated in Figure 4.2.

Now that the triangles are curvilinear the connectivity matrix $\overline{\overline{\boldsymbol{T}}}$ must be expanded with extra information, first of all it is essential to know which kind of structure a given triangle is a part of, i.e. flat, cylindrical or spherical. Secondly there is specific information for each case that needs to be stored. The case with flat triangles is trivially easy, as it is the same as the Facet Method, so it is only the spherical and cylindrical cases that need to be analyzed further. Each case is treated separately in a subsection each, we need to find the position function $\boldsymbol{r}_k^{(\text{exact})}(u,v)$, the area A_k, and the surface unit vectors $\hat{\boldsymbol{t}}^{(1)}(u,v)$ and $\hat{\boldsymbol{t}}^{(2)}(u,v)$.

4.1.1 Triangle on a Sphere

Suppose that we have a curved triangle on a sphere of radius R[1] with a center in $\boldsymbol{r}_c$, which must be stored in the connectivity matrix. We know that the triangle is relatively small compared to the sphere, so we do not need to worry about the flat triangle intersecting $\boldsymbol{r}_c$ for example. Then the position on the sphere with a given $\boldsymbol{r}_k(u,v)$ can be found by

$$\boldsymbol{r}_k^{(exact)}(u,v) = R\frac{\boldsymbol{r}_k(u,v) - \boldsymbol{r}_c}{\|\boldsymbol{r}_k(u,v) - \boldsymbol{r}_c\|} + \boldsymbol{r}_c. \tag{4.2}$$

[1]The radius is usually designated as a, but this is not the case for this subsection.

Finding the area of the curved triangle is more involved, but it can still be found analytically with the help of spherical trigonometry[7, 8]. The following formulas are based on spherical triangles on a unit sphere, so the distances involved need to be scaled up or down by a factor of R. It turns out that the area can be found by

$$A_k = R^2 E, \qquad \text{where} \qquad E = (A + B + C)/2, \tag{4.3}$$

E is called the spherical excess, where the angles A, B and C are defined as in Figure 4.3. The angles can be determined by using the arclengths a, b and c. Say that the angle at $\boldsymbol{r}_1$ is A, then the arclength a can be found by

$$a = \operatorname{acos}\left(\frac{\boldsymbol{r}_2 \cdot \boldsymbol{r}_3}{R^2}\right), \tag{4.4}$$

b and c can be found in a similar way. Now the semi-perimeter can be introduced $s = (a + b + c)/2$, and the half angle tangent formulas can be written as

$$\begin{aligned}
\tan(A/2) &= \frac{k}{\sin(s-a)} \\
\tan(B/2) &= \frac{k}{\sin(s-b)} \\
\tan(C/2) &= \frac{k}{\sin(s-c)},
\end{aligned}$$

where

$$k^2 = \frac{\sin(s-a)\sin(s-b)\sin(s-c)}{sin(s)}.$$

This is all that is needed to find the area of a spherical triangle.

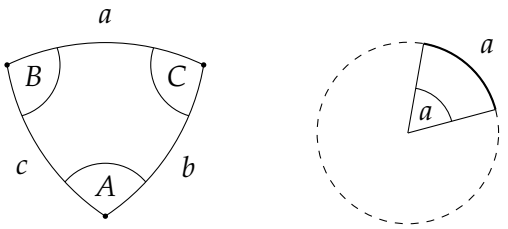

Figure 4.3: Notation for a spherical triangle on a unit sphere. The vertices are named A, B and C, the angles at these vertices are also named A, B and C. The arclengths a, b and c are also angles albeit an angle as seen from the center of the unit sphere as shown on the right.

The normal vector can easily be found by $\hat{\boldsymbol{n}}_k = \frac{\boldsymbol{r}_k^{(\text{exact})} - \boldsymbol{r}_c}{\left\| \boldsymbol{r}_k^{(\text{exact})} - \boldsymbol{r}_c \right\|}$. In spherical coordinates we have $\hat{\boldsymbol{n}}_k = \hat{\boldsymbol{r}}$, where $\hat{\boldsymbol{r}} = \sin\theta\cos\varphi\hat{\boldsymbol{x}} + \sin\theta\sin\varphi\hat{\boldsymbol{y}} + \cos\theta\hat{\boldsymbol{z}}$. The basis vector $\hat{\boldsymbol{t}}_k^{(1)}$ can be in any direction that is perpendicular to $\hat{\boldsymbol{n}}_k$, we can choose $\hat{\boldsymbol{\varphi}} = -\sin\varphi\hat{\boldsymbol{x}} + \cos\varphi\hat{\boldsymbol{y}}$. If the normal vector is $\hat{\boldsymbol{n}}_k = n_x\hat{\boldsymbol{x}} + n_y\hat{\boldsymbol{y}} + n_z\hat{\boldsymbol{z}}$ then the polar angle is $\theta = \operatorname{acos} n_z$, and finally we have $\hat{\boldsymbol{t}}_k^{(1)} = -\frac{n_y}{\sin\theta}\hat{\boldsymbol{x}} + \frac{n_x}{\sin\theta}\hat{\boldsymbol{y}}$. Now the last basis vector can be found based on the former two as usual, $\hat{\boldsymbol{t}}_k^{(2)} = \hat{\boldsymbol{t}}_k^{(1)} \times \hat{\boldsymbol{n}}_k = \hat{\boldsymbol{\theta}}$.

4.1.2 Triangle on a Cylinder

We have a curved triangle on a cylinder with radius a, the cylinder is symmetrical around a line that goes through $\boldsymbol{r}_c$ and is parallel with $\hat{\boldsymbol{n}}_c$, these unit vectors are stored in the connectivity matrix. The vertices intersect with the surface, but the other points on the flat triangle are a short distance away from the exact surface. Say we have a position $\boldsymbol{r}_k$ on the flat triangle then the corresponding position on the surface of the cylinder $\boldsymbol{r}_k^{(\text{exact})}$ can be found. To accomplish this the vector $\boldsymbol{r}_k - \boldsymbol{r}_c$ needs to be composed into a part that is parallel with the symmetry axis and a part that is perpendicular to it. These components are illustrated in Figure 4.4 and are defined by

$$\begin{aligned} \boldsymbol{r}_V &= \hat{\boldsymbol{n}}_c \left(\hat{\boldsymbol{n}}_c \cdot (\boldsymbol{r}_k - \boldsymbol{r}_c) \right), \\ \boldsymbol{r}_H &= \boldsymbol{r}_k - \boldsymbol{r}_c - \boldsymbol{r}_V. \end{aligned}$$

Then $\boldsymbol{r}_k^{(\text{exact})}$ can be found by

$$\boldsymbol{r}_k^{(\text{exact})} = \boldsymbol{r}_c + \boldsymbol{r}_V + a\frac{\boldsymbol{r}_H}{\|\boldsymbol{r}_H\|}. \tag{4.5}$$

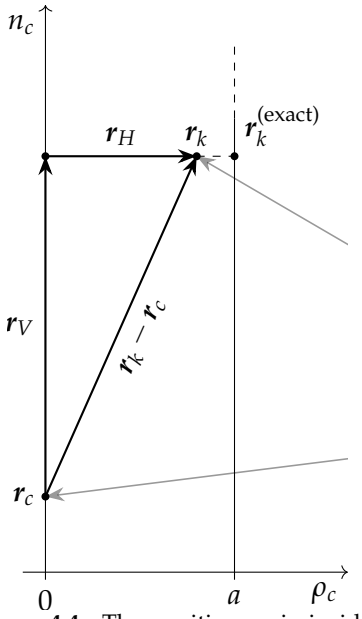

Figure 4.4: The position $\boldsymbol{r}_k$ is inside a cylinder of radius a and is a short distance from the surface. The closest position on the surface is called $\boldsymbol{r}_k^{(\text{exact})}$ and it is the desired quantity.

The area of the cylindrical triangle can be found by unraveling the surface of the cylinder into a 2D plane, as shown in Figure 4.5. The three vertices are given by $\boldsymbol{r}_i' = \boldsymbol{r}_{i,k} - \boldsymbol{r}_c$, where $i = 1, 2, 3$, these points can be written in cylindrical surface coordinates as $\boldsymbol{r}_i' = (\varphi_i, z_i)$. The vertical component is given by $z_i = \hat{\boldsymbol{n}}_c \cdot \boldsymbol{r}_i'$. The angle at $\boldsymbol{r}_1'$ is chosen to be zero, $\varphi_1 = 0$, then the other angles φ_2 and φ_3 can be determined in relation to it. In order to do this an in plane vector needs to be defined such that $\boldsymbol{v}_i = \boldsymbol{r}_i' - \hat{\boldsymbol{n}}_c z_i = a\begin{bmatrix}\cos\varphi_i & \sin\varphi_i & 0\end{bmatrix}^T$. It is important to consider

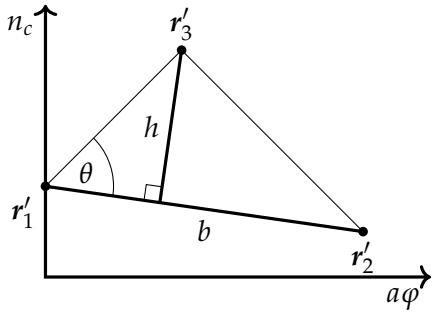

Figure 4.5: The triangle in a cylindrical surface coordinate system.

the angle with sign and it should be in the range $(-\pi, \pi]$, to achieve this the function atan2(y, x) is used. The angle for $\boldsymbol{r}'_2$ can be found to be

$$\varphi_2 = \text{atan2}\left((\boldsymbol{v}_1 \times \boldsymbol{v}_2) \cdot \hat{\boldsymbol{n}}_c, \boldsymbol{v}_1 \cdot \boldsymbol{v}_2\right), \tag{4.6}$$

the angle for $\boldsymbol{r}'_3$ can be found analogously. Now the area can easily be found by $A = bh/2$, where the base b and the height h are given by

$$b = \sqrt{(a\varphi_2)^2 + (z_2 - z_1)^2} \tag{4.7}$$

$$h = \sqrt{(a\varphi_3)^2 + (z_3 - z_1)^2}\sin\theta, \tag{4.8}$$

where the angle θ, which is also shown in Figure 4.5, can be found by

$$\theta = \text{acos}\left(\frac{a^2\varphi_2\varphi_3 + (z_2 - z_1)(z_3 - z_1)}{\sqrt{(a\varphi_2)^2 + (z_2 - z_1)^2}\sqrt{(a\varphi_3)^2 + (z_3 - z_1)^2}}\right). \tag{4.9}$$

The normal vector can be found by $\hat{\boldsymbol{n}}_k = \frac{\boldsymbol{r}_H}{\|\boldsymbol{r}_H\|}$, the first surface basis vector can aptly be chosen to be $\hat{\boldsymbol{t}}_k^{(1)} = \hat{\boldsymbol{n}}_c$, the second vector can be found in the usual way $\hat{\boldsymbol{t}}_k^{(2)} = \hat{\boldsymbol{t}}_k^{(1)} \times \hat{\boldsymbol{n}}_k$.

4.2 Subdivision

The centroidal approximation is as simple as before, it can still be found by using (3.10), except the center points, the basis vectors and the area need to be replaced by their exact equivalents. For example the exact observation point can be found by $\boldsymbol{s}_i = \boldsymbol{r}_i^{(\text{exact})}(u = 1/3, v = 1/3)$. The centroidal approximation is of course an approximation, in reality an integral should be carried out over the area of triangle k to find an element in the $\overline{\overline{\boldsymbol{K}}}$ matrices. The integral can be carried out with the help of the triangular coordinates in the following way

$$K_{ik}^{(m,n)} = P\int_{u=0}^{1}\int_{v=0}^{1-u} \hat{\boldsymbol{t}}_i^{(m)} \cdot \left[\hat{\boldsymbol{n}} \times \left[\boldsymbol{\nabla} \times \overleftrightarrow{G}\left(\boldsymbol{s}_i, \boldsymbol{r}_k^{(\text{exact})}(u, v)\right)\right]\right] \cdot \hat{\boldsymbol{t}}_k^{(n)}(u, v) 2\tilde{A}_k dv\, du, \tag{4.10}$$

where $\tilde{A}_k$ is the differential area,

$$\tilde{A}_k = \frac{1}{2}\left\| \frac{\partial \boldsymbol{r}_k(u,v)}{\partial u} \times \frac{\partial \boldsymbol{r}_k(u,v)}{\partial v} \right\|, \tag{4.11}$$

note that performing this integral over the whole domain still assumes that the current is constant in the domain. Performing this integral takes a large amount of time and it is hard to implement, this leads to the motivation for finding a compromise between these two approaches. Instead of just choosing one point in triangle k, $\boldsymbol{s}_k$, a number of points could be chosen $\boldsymbol{s}_k^{(q)}$. The points should ideally be evenly spread and each should have an associated surrounding area $A_k^{(q)}$, such that $\sum_q A_k^{(q)} = A_k$. For each point there is also a set of surface basis vectors $\hat{\boldsymbol{t}}_k^{(1,q)}$ and $\hat{\boldsymbol{t}}_k^{(2,q)}$.

One way to achieve this is to subdivide the u and v domain into N_{sub}^2 equal smaller subdomains as shown in Figure 4.6, then the subdivision scheme can be applied to all triangles, no matter if they are a part of a sphere or something else. Each dot in the figure is a u, v coordinate: $(u^{(q)}, v^{(q)})$ and the points in the k'th triangle can be found by $\boldsymbol{s}_k^{(q)} = \boldsymbol{r}_k^{(exact)}(u^{(q)}, v^{(q)})$ for $q = 1$ to N_{sub}^2. The sub-triangles in the u, v domain are also triangles in the real domain, which is important as we saw in the previous section how to calculate the area of a triangle on a sphere and cylinder, note that the area of the sub-triangles are not generally equal. Now we are ready to replace the centroidal approximation with what we can call the subdivision approximation:

$$K_{ik}^{(m,n)} \approx \sum_{q=1}^{N_{sub}^2} \hat{\boldsymbol{t}}_i^{(m)} \cdot \left[\hat{\boldsymbol{n}} \times \left[\boldsymbol{\nabla} \times \overleftrightarrow{G}\left(\boldsymbol{s}_i, \boldsymbol{s}_k^{(q)} \right) \right] \right] \cdot \hat{\boldsymbol{t}}_k^{(n,q)} A_k^{(q)}, \qquad \text{for} \qquad \boldsymbol{s}_k^{(q)} \neq \boldsymbol{s}_i, \tag{4.12}$$

the self-terms lead to the inequality condition on the right. The problem arises when $\boldsymbol{s}_k^{(q)} = \boldsymbol{s}_i$, because then Green's tensor becomes singular. The K elements are principal integrals, and we saw in the case of flat triangle that the self-term principal integral becomes zero, but this does not generally hold for a curvilinear triangle. In the case when N_{sub} is divisible by 3, then the observation point at $(u = 1/3, v = 1/3)$ does not coincide with $(u^{(q)}, v^{(q)})$ for any q, which can be seen in Figure 4.6, thus the subdivision approximation can be carried out without modification. In the case where N_{sub} is not divisible by 3, then the observation point does coincide with a subdivision point, the procedure is to say that the subdomain around the observation point is roughly flat and therefore the principal integral gives zero. Thus we have found an expression for the subdivision approximation, note that if $N_{sub} = 1$, then it is simply the centroidal approximation.

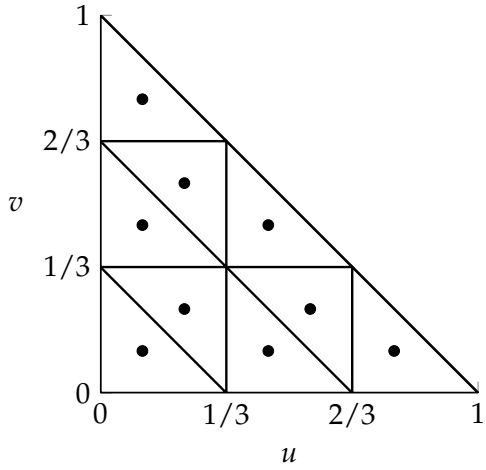

Figure 4.6: Illustration of the subdivision of the triangle domain into N_{sub}^2 smaller subdomains, here $N_{sub} = 3$. Each filled circle corresponds to a coordinate $(u^{(q)}, v^{(q)})$, such that $\boldsymbol{s}_k^{(q)} = \boldsymbol{r}_k(u^{(q)}, v^{(q)})$, where $q = 1$ to N_{sub}^2. Each coordinate is in the center of a subtriangle with an area of $A_k^{(q)}$, of course the area is for the real triangle and not in the u, v domain.

4.3 Facet and Curvilinear Method Comparison

In this section we will see how well the Curvilinear Method compares to the Facet Method by looking at the absolute error for a sphere compared to the results of the previous chapter. First the methods will be compared without subdivision, and then the effects of subdivision will be explored afterwards. The error is calculated on the basis of (3.12) as before.

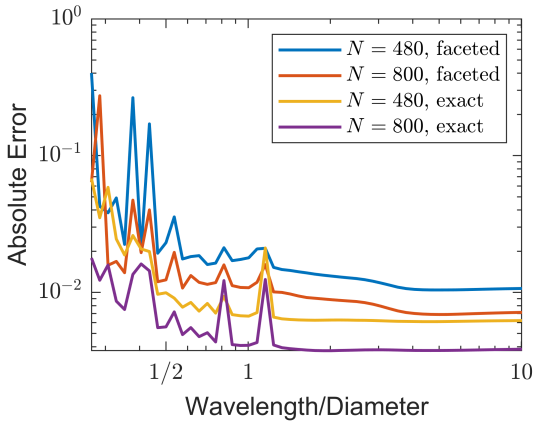

Figure 4.7: Comparison of the error for a sphere between the Facet Method (faceted) and the Curvilinear Method (exact). The comparison is based on calculation without subdivision, i.e. $N_{sub} = 1$.

By comparing the Facet Method to the Curvilinear Method as shown in Figure

4.7, we can see that the Curvilinear method is better across practically all wavelengths. In fact the Curvilinear Method produces better results at $N = 480$ than the Facet Method does at $N = 800$, this means that the Curvilinear Method is much faster and less memory intensive for a result with a given error. It also turns out that the CM is barely slower for a given N, for the case in Figure 4.7 it took on average 32.08s for the FM and 32.97s per wavelength for $N = 800$.In conclusion we can see that there are large gains for implementing a method that represents the scatterer surface accurately.

Next we will see how subdivision changes the error, the subdivision can apply

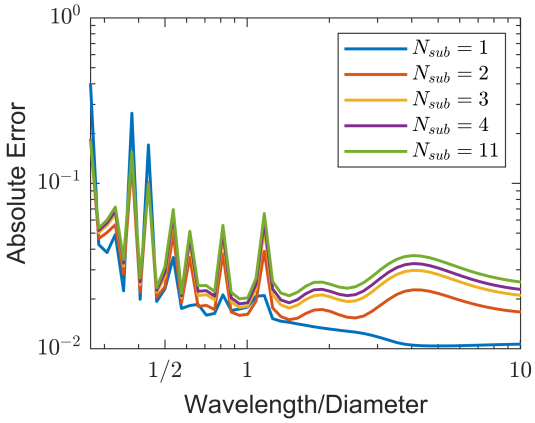

Figure 4.8: The absolute error F for the Facet Method with $N = 480$ and a varied degree of subdivision, $N_{sub} = 1$ corresponds to no subdivision.

to the FM just as well as the CM. However, there are some limits to the FM in this regard, because the normal vector does not change depending on the location within a given triangle, so the direction of the surface vector does not change as it does in the CM. The Error for the FM with and without subdivision is shown in Figure 4.8, and we can see that the error becomes worse as the triangles are subdivided more finely, i.e. N_{sub} increases. This is a surprising result as the subdivision approximation is supposed to be more accurate than the centriodal approximation, it seems that the problems with the faceted surface are enhanced with the subdivision approximation.

Fortunately we can see in Figure 4.9 that the subdivision is much better for the CM, although it is not uniformly better. The result for $N = 480$ and $N = 800$ are functionally identical, so the following discussion fits equally well for either plot. The error quickly converges for $N_{sub} > 0$, and we can see that the error for $N_{sub} = 4$ and $N_{sub} = 11$ is almost equal, so there is seemingly no reason to pick a N_{sub} higher than 4. The fact that it converges for small degree of subdivision suggests that there is not a large benefit to be gained from performing the full integrals. The case with $N_{sub} = 3$, is slightly worse than the others, but it is also calculated slightly differently as we saw in section 4.2, so it is best to avoid a N_{sub}

that is divisible by 3.

Interestingly the error is larger for small wavelength when there is subdivision, and that holds true for $N = 480$ and $N = 800$. Furthermore there is an additional peak at $\lambda \approx 0.8D$ after subdivision, and the peak at $\lambda \approx 1.2D$ is unaffected by subdivision. On the other hand the error is much lower for large wavelengths, the error with $N_{sub} = 4$ compared $N_{sub} = 1$ at $\lambda = 10D$ is just a quarter for $N = 480$ and a fifth for $N = 800$. Clearly is an effective method for reducing the error, at least when the wavelength is large, in this case the subdivision approximation is as good as or better than the centroidal approximation when $\lambda > D$. The reason the subdivision approximation is worse for small wavelengths is like due to the fact that the current is assumed constant over each triangle, it is also possible to model the current as linearly or quadratically varying across each triangle, but that is outside the scope of this project.

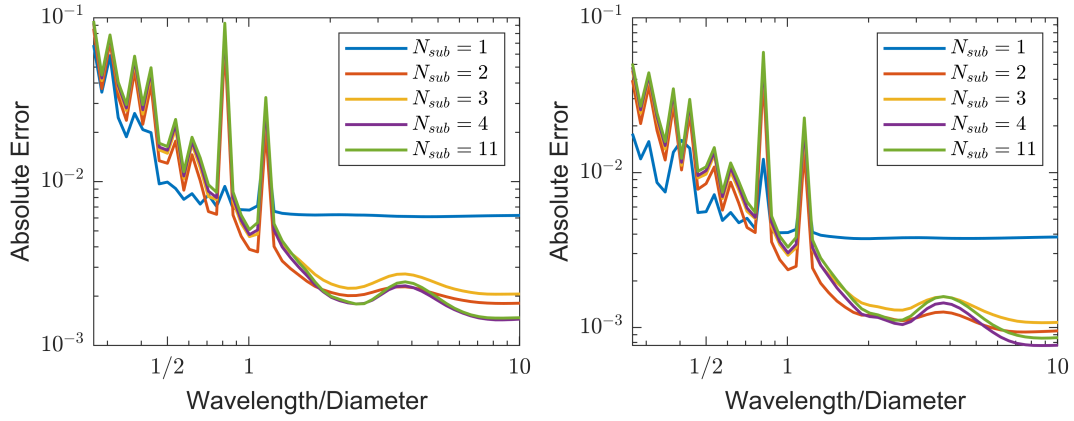

(a) $N = 480$ **(b)** $N = 800$

Figure 4.9: The error for the Curvilinear Method with **(a)** $N = 480$ and **(b)** $N = 800$, with a number of N_{sub}.

4.4 Calculations for a Rod

Now we have seen that the CM works for a sphere, in this section we will see if the model also works for a scatterer that is a composite of spherical and cylindrical segments. A simple rod is chosen for this task, which is a cylinder with two end caps in the form of half-spheres, the radius is $a = 10$nm and the total length is $L = 100$nm. There is no analytical solution for this case but we can make an educated guess, and the CM can also be compared to another GFSIEM model that uses cylindrical symmetry. The incident light is assumed to be polarized along the length of the rod, then in the thin wire approximation ($a << L$) the peaks of the scattering cross section should lie around $L = 2\lambda$, $\frac{3}{2}\lambda$, $\frac{5}{2}\lambda$ and so on, in this case $\lambda = 200$nm, 66.67nm, 40nm.

The scattering cross sections for the rod as calculated with the CM and the GF-SIEM that uses cylindrical symmetry are plotted in Figure 4.10. We can see that the models are roughly in agreement, and the peaks around 70nm and 240nm are slightly above the first guess of 67nm and 200nm. The model based on cylindrical symmetry is still a numerical model, and it is based on an approximation that can underestimate the scattering cross section, especially at the low wavelengths. Thus there is good reason to be optimistic about the CM when it comes to low wavelengths, as it also seems to have converged. However the CM has not converged near the 240nm peak, this is a surprising result compared to the previous section as there the error went drastically down as the wavelength increased. The scattering cross section must be highly sensitive to the current, which could be modeled as linearly or quadratically varying across each triangle instead of being constant, however that is outside the scope of this project. Modeling the current as linearly varying would not be a trivial addition to the CM, because the sampling points should be at the corner points rather than the center points.

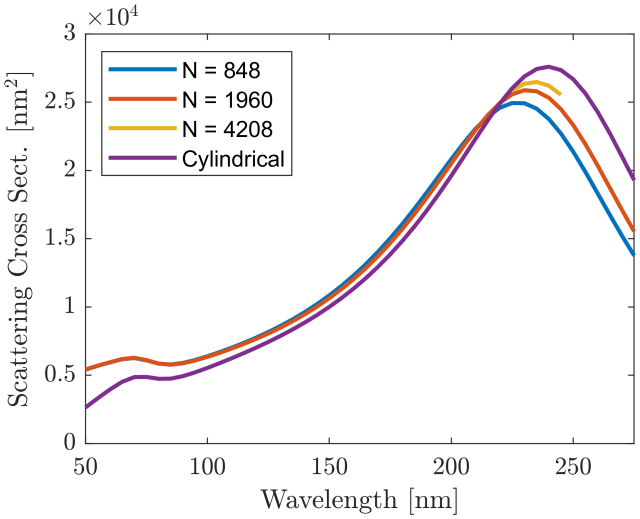

Figure 4.10: Scattering cross section for a rod with length $L = 100$nm and radius $a = 10$nm, the incident light is polarized along the length of the rod. The scattering is modeled by the Curvilinear Method with $N = 848$, 1960, 4208 with $N_{sub} = 4$, and by a GFSIEM method that uses cylindrical symmetry, it expands the electric field into cylindrical harmonics, the model only considers the 0'th order harmonic. Note that the case with $N = 4208$ is only plotted for a short interval 235nm to 245nm.

Chapter 5

Scatterer Near a Planar Interface

So far we have looked at a scatterer in free space in this chapter we will see how to update the model to accommodate an interface.

The reference dielectic constant is given by

$$\varepsilon_{\text{ref}}(\boldsymbol{r}) = \begin{cases} \varepsilon_1 & \text{for} \quad z > 0 \\ \varepsilon_2 & \text{for} \quad z < 0, \end{cases} \tag{5.1}$$

unless otherwise specified ε_i is assumed to be real, i.e. lossless, and positive.
If a plane wave with propagation vector $\boldsymbol{k}_1$ is incident on an interface, then part of it will be reflected and part of it is transmitted as illustrated on Figure 5.1. The incident, reflected and transmitted waves all travel in the same plane called the plane of incidence, which is spanned by $\hat{\boldsymbol{\rho}}$ and $\hat{\boldsymbol{z}}$ in the Figure, where the usual cylindrical coordinates are used:

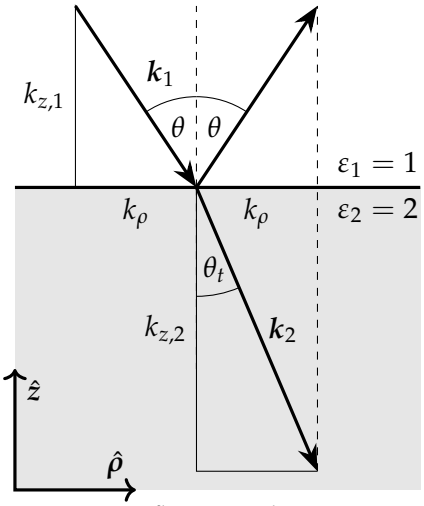

Figure 5.1: Reflection and transmission at a planar interface. The propagation vector $\boldsymbol{k}_1$ can be split into a vertical component $k_{z,1}$ and an in-plane component $k_\rho = \sqrt{k_x^2 + k_y^2}$. The propagation vector changes magnitude and direction across the interface, but the in-plane component is constant.

$$\hat{\boldsymbol{\rho}} = \quad \hat{\boldsymbol{x}} \cos\varphi + \hat{\boldsymbol{y}} \sin\varphi, \tag{5.2}$$

$$\hat{\boldsymbol{\varphi}} = -\hat{\boldsymbol{x}} \sin\varphi + \hat{\boldsymbol{y}} \cos\varphi. \tag{5.3}$$

The vector $\boldsymbol{k}_1$ can be split into a component along $\hat{\boldsymbol{z}}$ and a component along $\hat{\boldsymbol{\rho}}$ in the x, y-plane called $k_{z,1}$ and $k_\rho = \sqrt{k_x^2 + k_y^2}$ respectively (these are only magnitudes and do not account for direction). The magnitude of the propagation vectors is $k_i = k_0\sqrt{\varepsilon_i}$, but the in-plane component k_ρ is constant, this accounts for the change of direction across the interface. How much light is reflected and

transmitted can be determined by using Fresnel's coefficients, but they are dependent on the polarization of the light. The electric field is perpendicular to the propagation vector and is p-polarized if it is in the plane of incidence, and s-polarized if the field is perpendicular to the plane.
Finally the electric field can be written as

$$\boldsymbol{E}(\boldsymbol{r}) = \begin{cases} \left[\boldsymbol{E}_0 e^{-ik_{z,1}z} + \left[\boldsymbol{E}_0^{(s)} r^{(s)}(k_\rho) + \boldsymbol{E}_{0,r}^{(p)} r^{(p)}(k_\rho)\right] e^{ik_{z,1}z}\right] e^{ik_\rho \hat{\boldsymbol{\rho}}\cdot\boldsymbol{r}} & \text{for} \quad z > 0, \\ \left[\boldsymbol{E}_0^{(s)} t^{(s)}(k_\rho) + \boldsymbol{E}_{0,t}^{(p)} t^{(p)}(k_\rho)\right] e^{-ik_{z,2}z} e^{ik_\rho \hat{\boldsymbol{\rho}}\cdot\boldsymbol{r}} & \text{for} \quad z < 0, \end{cases} \tag{5.4}$$

where $\boldsymbol{E}_0^{(s)} = (\boldsymbol{E}_0 \cdot \hat{\boldsymbol{\varphi}})\hat{\boldsymbol{\varphi}} = E_0^{(s)}\hat{\boldsymbol{\varphi}}$ is the s-polarized part of the incident field. The p-polarized part changes direction depending on whether it is reflected or transmitted, hence the subscript r and t. The magnitude of the p-polarized part $E_0^{(p)}$ is defined such that $E_0^{(p)}\hat{\boldsymbol{k}}_1 \times \hat{\boldsymbol{\varphi}} = \boldsymbol{E}_0 - \boldsymbol{E}_0^{(s)}$. The p-polarized part of incident field for the reflected and transmitted light is given by $\boldsymbol{E}_{0,r}^{(p)} = E_0^{(p)}\hat{\boldsymbol{k}}_{1,r} \times \hat{\boldsymbol{\varphi}}$ and $\boldsymbol{E}_{0,t}^{(p)} = E_0^{(p)}\hat{\boldsymbol{k}}_2 \times \hat{\boldsymbol{\varphi}}$, where $\hat{\boldsymbol{k}}_{1,r}$ is the propagation vector for the reflected field, and it can easily be obtained from $\hat{\boldsymbol{k}}_1$ by changing the sign of the z-component. The Fresnel coefficients are given by

$$r^{(s)}(k_\rho) = \frac{k_{z,1} - k_{z,2}}{k_{z,1} + k_{z,2}} \qquad t^{(s)}(k_\rho) = 1 + r^{(s)}(k_\rho) \tag{5.5}$$

$$r^{(p)}(k_\rho) = \frac{\varepsilon_2 k_{z,1} - \varepsilon_1 k_{z,2}}{\varepsilon_2 k_{z,1} + \varepsilon_1 k_{z,2}} \qquad t^{(p)}(k_\rho) = 1 + r^{(p)}(k_\rho), \tag{5.6}$$

the coefficients describe the amplitude of the wave after reflection and transmission and also the phase change because it is a complex value. The coefficients are functions of k_ρ because $k_{z,i}$ is a given by

$$k_{z,i}(k_\rho) = \sqrt{k_0^2 \varepsilon_i - k_\rho^2}, \tag{5.7}$$

note that k_ρ can be larger than $k_0\sqrt{\varepsilon_i}$, even though it does not make much sense on the drawing, this makes $k_{z,i}$ an imaginary number and in turn makes $e^{ik_{z,i}z}$ exponentially decreasing. Far from the interface these fields will be non-existent, but in close they are important to consider.

5.1 Green's Functions for a Planar Interface

So far we have only looked at the case where there is only a direct contribution from a surface point $\boldsymbol{r}'$ to the observation point $\boldsymbol{r}$, but if there is a reflective interface then the point $\boldsymbol{r}'$ can also make an indirect contribution to the field at the observation point, as illustrated in Figure 5.2.

The total Green's tensor can be expressed as

$$\overleftrightarrow{G} = \begin{cases} \overleftrightarrow{G}^{(d)} + \overleftrightarrow{G}^{(i)} & \text{for} \quad z > 0 \\ \overleftrightarrow{G}^{(t)} & \text{for} \quad z < 0, \end{cases} \tag{5.8}$$

where $\overleftrightarrow{G}^{(d)}$ is the direct Green's tensor, and is equal to the usual tensor (2.15), the superscript (i) stands for indirect and (t) for the transmitted part. The tensors are found for a layered structure in [5, chapter 6], and they are given as an integral over the in-plane part of the propagation vector k_ρ. In order to do this, a cylindrical coordinate system must be introduced, which is also illustrated in Figure 5.2. We can see that each point $\boldsymbol{r}'$ becomes the origin of a new coordinate system, except the z-coordinate which is the same as in the Cartesian system. The vectors $\hat{\boldsymbol{\rho}}_{\boldsymbol{r}}$ and $\hat{\boldsymbol{\varphi}}_{\boldsymbol{r}}$ is defined as the normal cylindrical coordinates like (5.2) and (5.3), but they have the subscript r for *relative* as they change each time $\boldsymbol{r}'$ does. The relative horizontal distance ρ_r and the angle φ_r is defined by

$$x - x' = \rho_r \cos\varphi_r, \qquad y - y' = \rho_r \sin\varphi_r. \tag{5.9}$$

The benefit of introducing this coordinate system is to avoid the need to do a double integral over k_x and k_y.

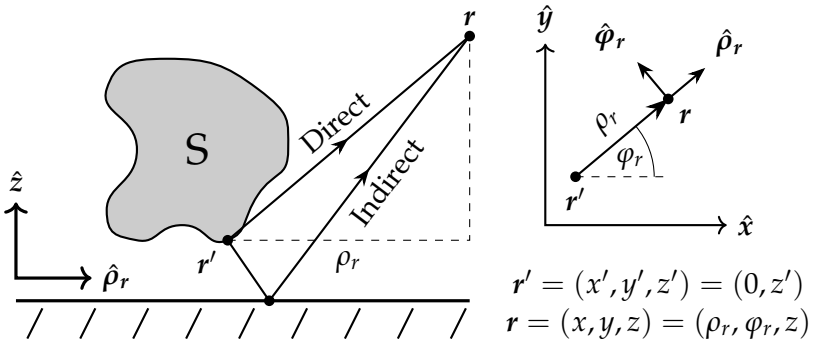

Figure 5.2: Illustration of the direct and indirect contribution from point $\boldsymbol{r}'$ to $\boldsymbol{r}$. A relative cylindrical coordinate system is introduced such that the plane of incidence is spanned by $\hat{\boldsymbol{\rho}}_{\boldsymbol{r}}$ and z and ρ_r is the horizontal distance between $\boldsymbol{r}'$ and $\boldsymbol{r}$.

As we have seen the Fresnel coefficients are different for s and p-polarized light, so the tensor needs to be split up into terms concerning either polarization, and then multiplied by the appropriate coefficient.
With that prelude we are ready to introduce the indirect Green's tensor, which is

defined as

$$\begin{aligned}\overleftrightarrow{G}^{(i)}(\boldsymbol{r},\boldsymbol{r}') =& \frac{i}{4\pi}\int_0^\infty \Bigg\{ r^{(p)}(k_\rho)\Bigg[\hat{\boldsymbol{z}}\hat{\boldsymbol{z}}\frac{k_\rho^2}{k_1^2}\mathrm{J}_0(k_\rho\rho_r) + \hat{\boldsymbol{\varphi}}_{\boldsymbol{r}}\hat{\boldsymbol{\varphi}}_{\boldsymbol{r}}\frac{k_{z,1}^2}{k_1^2}\frac{\mathrm{J}_0'(k_\rho\rho_r)}{k_\rho\rho_r} + \\ &\hat{\boldsymbol{\rho}}_{\boldsymbol{r}}\hat{\boldsymbol{\rho}}_{\boldsymbol{r}}\frac{k_{z,1}^2}{k_1^2}\mathrm{J}_0''(k_\rho\rho_r) - (\hat{\boldsymbol{z}}\hat{\boldsymbol{\rho}}_{\boldsymbol{r}} - \hat{\boldsymbol{\rho}}_{\boldsymbol{r}}\hat{\boldsymbol{z}})\frac{ik_\rho k_{z,1}}{k_1^2}\mathrm{J}_0'(k_\rho\rho_r)\Bigg] \\ &- r^{(s)}(k_\rho)\left[\hat{\boldsymbol{\varphi}}_{\boldsymbol{r}}\hat{\boldsymbol{\varphi}}_{\boldsymbol{r}}\mathrm{J}_0''(k_\rho\rho_r) + \hat{\boldsymbol{\rho}}_{\boldsymbol{r}}\hat{\boldsymbol{\rho}}_{\boldsymbol{r}}\frac{\mathrm{J}_0'(k_\rho\rho_r)}{k_\rho\rho_r}\right]\Bigg\}\frac{k_\rho}{k_{z,1}}e^{ik_{z,1}(z+z')}dk_\rho,\end{aligned} \tag{5.10}$$

where J_0 is the Bessel function of the first kind and zeroth order. If $\boldsymbol{r}'$ and/or $\boldsymbol{r}$ is not on the interface then $e^{ik_{z,1}(z+z')}$ will be an exponentially decreasing function when $k_\rho > k_1$, which makes it possible to integrate $\overleftrightarrow{G}^{(i)}$ numerically, and if either point is far enough away, then it is sufficient to integrate to k_1. However, if $\boldsymbol{r}'$ and $\boldsymbol{r}$ is on the interface then $\overleftrightarrow{G}^{(i)}$ is a singularity that we need to integrate over analytically, this will be the subject of the next section. The transmitted Green's tensor is given by

$$\begin{aligned}\overleftrightarrow{G}^{(t)}(\boldsymbol{r},\boldsymbol{r}') =& \frac{i}{4\pi}\int_0^\infty \Bigg\{ t^{(p)}(k_\rho)\frac{\varepsilon_1}{\varepsilon_2}\Bigg[\hat{\boldsymbol{z}}\hat{\boldsymbol{z}}\frac{k_\rho^2}{k_1^2}\mathrm{J}_0(k_\rho\rho_r) - \hat{\boldsymbol{\varphi}}_{\boldsymbol{r}}\hat{\boldsymbol{\varphi}}_{\boldsymbol{r}}\frac{k_{z,1}k_{z,2}}{k_1^2}\frac{\mathrm{J}_0'(k_\rho\rho_r)}{k_\rho\rho_r} - \\ &\hat{\boldsymbol{\rho}}_{\boldsymbol{r}}\hat{\boldsymbol{\rho}}_{\boldsymbol{r}}\frac{k_{z,1}k_{z,2}}{k_1^2}\mathrm{J}_0''(k_\rho\rho_r) - \left(\hat{\boldsymbol{z}}\hat{\boldsymbol{\rho}}_{\boldsymbol{r}} + \hat{\boldsymbol{\rho}}_{\boldsymbol{r}}\hat{\boldsymbol{z}}\frac{k_{z,2}}{k_{z,1}}\right)\frac{ik_\rho k_{z,1}}{k_1^2}\mathrm{J}_0'(k_\rho\rho_r)\Bigg] \\ &- t^{(s)}(k_\rho)\left[\hat{\boldsymbol{\varphi}}_{\boldsymbol{r}}\hat{\boldsymbol{\varphi}}_{\boldsymbol{r}}\mathrm{J}_0''(k_\rho\rho_r) + \hat{\boldsymbol{\rho}}_{\boldsymbol{r}}\hat{\boldsymbol{\rho}}_{\boldsymbol{r}}\frac{\mathrm{J}_0'(k_\rho\rho_r)}{k_\rho\rho_r}\right]\Bigg\}\frac{k_\rho}{k_{z,1}}e^{ik_{z,1}z'}e^{-ik_{z,2}z}dk_\rho.\end{aligned} \tag{5.11}$$

The magnetic GFSIEM is used to find the current on the surface as before, this means that we need to find the curl of the indirect Green's tensor. Curl in cylindrical coordinates is

$$\nabla\times\overleftrightarrow{G}^{(i)} = \hat{\boldsymbol{z}}\times\frac{\partial\overleftrightarrow{G}^{(i)}}{\partial z} + \hat{\boldsymbol{\varphi}}_{\boldsymbol{r}}\times\frac{1}{\rho_r}\frac{\partial\overleftrightarrow{G}^{(i)}}{\partial\varphi_r} + \hat{\boldsymbol{\rho}}_{\boldsymbol{r}}\times\frac{\partial\overleftrightarrow{G}^{(i)}}{\partial\rho_r}. \tag{5.12}$$

The only terms in $\overleftrightarrow{G}^{(i)}$ that are dependent on φ_r are the unit vectors

$$\frac{\partial\hat{\boldsymbol{\rho}}_{\boldsymbol{r}}}{\partial\varphi_r} = \hat{\boldsymbol{\varphi}}_{\boldsymbol{r}}, \qquad \frac{\partial\hat{\boldsymbol{\varphi}}_{\boldsymbol{r}}}{\partial\varphi_r} = -\hat{\boldsymbol{\rho}}_{\boldsymbol{r}}, \tag{5.13}$$

no unit-vector is dependent on either ρ_r or z. The derivation of $\boldsymbol{\nabla}\times\overleftrightarrow{G}^{(i)}$ is straight-

forward but lengthy, here is an example of taking the curl of one term:

$$\nabla \times \left[\hat{\boldsymbol{\varphi}}_{\boldsymbol{r}}\hat{\boldsymbol{\varphi}}_{\boldsymbol{r}}\frac{\mathrm{J}_0'(k_\rho\rho_r)}{k_\rho\rho_r}e^{ik_{z,1}(z+z')}\right] = \Bigg[-\hat{\boldsymbol{\rho}}_{\boldsymbol{r}}\hat{\boldsymbol{\varphi}}_{\boldsymbol{r}}\frac{\mathrm{J}_0'(k_\rho\rho_r)}{k_\rho\rho_r}ik_{z,1} + \hat{\boldsymbol{z}}\hat{\boldsymbol{\varphi}}_{\boldsymbol{r}}\frac{1}{\rho_r}\frac{\mathrm{J}_0'(k_\rho\rho_r)}{k_\rho\rho_r} + \hat{\boldsymbol{z}}\hat{\boldsymbol{\varphi}}_{\boldsymbol{r}}\left(-\frac{1}{\rho_r}\frac{\mathrm{J}_0'(k_\rho\rho_r)}{k_\rho\rho_r} + \frac{\mathrm{J}_0''(k_\rho\rho_r)}{\rho_r}\right)\Bigg]e^{ik_{z,1}(z+z')}. \tag{5.14}$$

In total the curl is given by the following equation

$$\boldsymbol{\nabla}\times\overleftrightarrow{\mathrm{G}}^{(i)}(\boldsymbol{r},\boldsymbol{r}') = \frac{i}{4\pi}\int_0^\infty \Bigg\{ r^{(p)}(k_\rho)\left[-\hat{\boldsymbol{\varphi}}_{\boldsymbol{r}}\hat{\boldsymbol{z}}\,k_\rho\mathrm{J}_0'(k_\rho\rho_r) + \hat{\boldsymbol{\varphi}}_{\boldsymbol{r}}\hat{\boldsymbol{\rho}}_{\boldsymbol{r}}\,ik_{z,1}\mathrm{J}_0''(k_\rho\rho_r) - \hat{\boldsymbol{\rho}}_{\boldsymbol{r}}\hat{\boldsymbol{\varphi}}_{\boldsymbol{r}}\,ik_{z,1}\frac{\mathrm{J}_0'(k_\rho\rho_r)}{k_\rho\rho_r}\right] - r^{(s)}(k_\rho)\left[-\hat{\boldsymbol{z}}\hat{\boldsymbol{\varphi}}_{\boldsymbol{r}}\,k_\rho\mathrm{J}_0'(k_\rho\rho_r) + \hat{\boldsymbol{\varphi}}_{\boldsymbol{r}}\hat{\boldsymbol{\rho}}_{\boldsymbol{r}}\,ik_{z,1}\frac{\mathrm{J}_0'(k_\rho\rho_r)}{k_\rho\rho_r} - \hat{\boldsymbol{\rho}}_{\boldsymbol{r}}\hat{\boldsymbol{\varphi}}_{\boldsymbol{r}}\,ik_{z,1}\mathrm{J}_0''(k_\rho\rho_r)\right]\Bigg\}\frac{k_\rho}{k_{z,1}}e^{ik_{z,1}(z+z')}\,dk_\rho, \tag{5.15}$$

now we just need to find out what happens in the singularity.

5.2 Singularity

The singularity of $\hat{\boldsymbol{n}}\times\boldsymbol{\nabla}\times\overleftrightarrow{\mathrm{G}}^{(i)}(\boldsymbol{r}',\boldsymbol{r})\cdot\boldsymbol{J}$ for an observation point on the interface need to be dealt with analytically. First we evaluate the singular part of the k_ρ integral and then integrate over an infinitesimal area ∂S around the observation point.

We have $\boldsymbol{r}'\to\boldsymbol{r}$, where $\boldsymbol{r}$ is on the bottom of the scatterer which approaches the interface, this means that $(z+z')\to 0$ and $\rho_r\to 0$. We assume that the scatterer is smooth, therefore ∂S will be flat and the current is in the x,y-plane: $\boldsymbol{J}=\hat{\boldsymbol{x}}J_x+\hat{\boldsymbol{y}}J_y$, also the normal vector is given by $\hat{\boldsymbol{n}}=-\hat{\boldsymbol{z}}$. Since we are interesting in finding $\hat{\boldsymbol{n}}\times\boldsymbol{\nabla}\times\overleftrightarrow{\mathrm{G}}^{(i)}(\boldsymbol{r},\boldsymbol{r}')\cdot\boldsymbol{J}$ we can ignore the terms that contain $\hat{\boldsymbol{z}}$. We need to find the asymptotic behavior of the integrand for large k_ρ, because it is this part that makes the integral singular. The Fresnel coefficients can be found for large k_ρ by first making this approximation:

$$k_{z,i} = ik_\rho\sqrt{1-\frac{k_0^2\varepsilon_i}{k_\rho^2}} \approx ik_\rho\left(1-\frac{1}{2}\frac{k_0^2\varepsilon_i}{k_\rho^2}\right), \tag{5.16}$$

then the Fresnel coefficients approximate to

$$r^{(p)}(k_\rho)\approx\frac{\varepsilon_2-\varepsilon_1}{\varepsilon_2+\varepsilon_1} \qquad r^{(s)}(k_\rho)\approx\frac{1}{k_\rho^2}\frac{k_0^2}{4}(\varepsilon_2-\varepsilon_1), \tag{5.17}$$

thus only the p-polarized terms lead to a singularity. We can approximate $k_{z,1}$ further For very large k_ρ: $k_{z,1} \approx ik_\rho$, thus the singular part of the indirect tensor is

$$\hat{\boldsymbol{n}} \times \boldsymbol{\nabla} \times \overset{\leftrightarrow}{G}^{(i)}(\boldsymbol{r}, \boldsymbol{r'}) \cdot \boldsymbol{J} \approx$$
$$\overset{\leftrightarrow}{T} = -\frac{1}{4\pi}\frac{\varepsilon_2 - \varepsilon_1}{\varepsilon_2 + \varepsilon_1}\int_0^\infty \left\{ \hat{\boldsymbol{\rho}}_{\boldsymbol{r}}\hat{\boldsymbol{\rho}}_{\boldsymbol{r}} k_\rho \mathrm{J}_0''(k_\rho\rho_r) - \hat{\boldsymbol{\varphi}}_{\boldsymbol{r}}\hat{\boldsymbol{\varphi}}_{\boldsymbol{r}} \frac{\mathrm{J}_0'(k_\rho\rho_r)}{\rho_r} \right\} e^{-k_\rho(z+z')} dk_\rho \cdot \boldsymbol{J}, \quad (5.18)$$

where it has been called $\overset{\leftrightarrow}{T}$ for later convenience. The derivatives of the Bessel function can be expressed in terms of other Bessel functions:

$$\mathrm{J}_0'(x) = -\mathrm{J}_1(x), \qquad \mathrm{J}_0''(x) = -\mathrm{J}_0(x) + \frac{1}{x}\mathrm{J}_1(x). \quad (5.19)$$

Now we need a couple of formulas that can for example be found in [6]:

$$\int_0^\infty \mathrm{J}_0(k_\rho\rho_r) e^{-k_\rho(z+z')} dk_\rho = \frac{1}{\tilde{R}}, \quad (5.20)$$
$$\int_0^\infty \mathrm{J}_1(k_\rho\rho_r) e^{-k_\rho(z+z')} dk_\rho = \frac{\tilde{R} - (z+z')}{\rho_r \tilde{R}}, \quad (5.21)$$

where $\tilde{R} = \sqrt{\rho_r^2 + (z+z')^2}$. Now we have what we need to evaluate the integral

$$\begin{aligned}
\overset{\leftrightarrow}{T} &= -\frac{1}{4\pi}\frac{\varepsilon_2 - \varepsilon_1}{\varepsilon_2 + \varepsilon_1}\int_0^\infty \left\{ -\hat{\boldsymbol{\rho}}_{\boldsymbol{r}}\hat{\boldsymbol{\rho}}_{\boldsymbol{r}} k_\rho \mathrm{J}_0(k_\rho\rho_r) + (\hat{\boldsymbol{\rho}}_{\boldsymbol{r}}\hat{\boldsymbol{\rho}}_{\boldsymbol{r}} - \hat{\boldsymbol{\varphi}}_{\boldsymbol{r}}\hat{\boldsymbol{\varphi}}_{\boldsymbol{r}}) \frac{\mathrm{J}_1(k_\rho\rho_r)}{\rho_r} \right\} e^{-k_\rho(z+z')} dk_\rho \cdot \boldsymbol{J} \\
&= -\frac{1}{4\pi}\frac{\varepsilon_2 - \varepsilon_1}{\varepsilon_2 + \varepsilon_1}\left\{ -\hat{\boldsymbol{\rho}}_{\boldsymbol{r}}\hat{\boldsymbol{\rho}}_{\boldsymbol{r}} \frac{z+z'}{\tilde{R}^3} + (\hat{\boldsymbol{\rho}}_{\boldsymbol{r}}\hat{\boldsymbol{\rho}}_{\boldsymbol{r}} - \hat{\boldsymbol{\varphi}}_{\boldsymbol{r}}\hat{\boldsymbol{\varphi}}_{\boldsymbol{r}}) \frac{\tilde{R} - (z+z')}{\rho_r^2 \tilde{R}} \right\} \cdot \boldsymbol{J} \\
&= \frac{1}{4\pi}\frac{\varepsilon_2 - \varepsilon_1}{\varepsilon_2 + \varepsilon_1}\left\{ (\hat{\boldsymbol{\rho}}_{\boldsymbol{r}}\hat{\boldsymbol{\rho}}_{\boldsymbol{r}} + \hat{\boldsymbol{\varphi}}_{\boldsymbol{r}}\hat{\boldsymbol{\varphi}}_{\boldsymbol{r}}) \frac{1}{2}\frac{z+z'}{\tilde{R}^3} \right. \\
&\qquad \left. + (\hat{\boldsymbol{\rho}}_{\boldsymbol{r}}\hat{\boldsymbol{\rho}}_{\boldsymbol{r}} - \hat{\boldsymbol{\varphi}}_{\boldsymbol{r}}\hat{\boldsymbol{\varphi}}_{\boldsymbol{r}}) \left(\frac{1}{2}\frac{z+z'}{\tilde{R}^3} - \frac{\tilde{R} - (z+z')}{\rho_r^2 \tilde{R}} \right) \right\} \cdot \boldsymbol{J},
\end{aligned}$$

where it has been used that

$$-k_\rho \mathrm{J}_0(k_\rho\rho_r) e^{-k_\rho(z+z')} = \frac{\partial}{\partial z}\left(\mathrm{J}_0(k_\rho\rho_r) e^{-k_\rho(z+z')} \right) \qquad \text{and} \qquad \frac{\partial}{\partial z}\left(\frac{1}{\tilde{R}} \right) = -\frac{z+z'}{\tilde{R}^3}.$$

We need to integrate around the observation point from $\varphi_r = 0$ to 2π, only the unit vectors are affected. The first term evaluates to something that is not dependent on φ_r as $(\hat{\boldsymbol{\rho}}_{\boldsymbol{r}}\hat{\boldsymbol{\rho}}_{\boldsymbol{r}} + \hat{\boldsymbol{\varphi}}_{\boldsymbol{r}}\hat{\boldsymbol{\varphi}}_{\boldsymbol{r}}) = (\hat{\boldsymbol{x}}\hat{\boldsymbol{x}} + \hat{\boldsymbol{y}}\hat{\boldsymbol{y}})$, however the other term needs to be integrated

$$\int_0^{2\pi} (\hat{\boldsymbol{\rho}}_{\boldsymbol{r}}\hat{\boldsymbol{\rho}}_{\boldsymbol{r}} - \hat{\boldsymbol{\varphi}}_{\boldsymbol{r}}\hat{\boldsymbol{\varphi}}_{\boldsymbol{r}}) d\varphi_r = \int_0^{2\pi} (\cos^2\varphi_r \hat{\boldsymbol{x}}\hat{\boldsymbol{x}} + \sin^2\varphi_r \hat{\boldsymbol{y}}\hat{\boldsymbol{y}} - \sin^2\varphi_r \hat{\boldsymbol{x}}\hat{\boldsymbol{x}} - \cos^2\varphi_r \hat{\boldsymbol{y}}\hat{\boldsymbol{y}}) d\varphi_r = 0,$$

thus only one term needs to be evaluated. The singularity is therefore given by

$$\int_{\partial S} \overleftrightarrow{T}\, dx'\, dy' = \frac{1}{4\pi}\frac{\varepsilon_2-\varepsilon_1}{\varepsilon_2+\varepsilon_1}\frac{\boldsymbol{J}}{2}\int_{\partial S}\frac{z+z'}{\tilde{R}^3}dx'\, dy', \tag{5.22}$$

the integral is equivalent to an integral over the solid angle as seen from a point $z+z'$ below the observation point, so $d\Omega = \frac{z+z'}{\tilde{R}^3}dx'\, dy'$. As z and z' approaches 0, the integral will correspond to the the area of half the unit sphere, i.e. 2π.

Finally the singularity can be evaluated to

$$\boxed{\int_{\partial S} \hat{\boldsymbol{n}} \times \boldsymbol{\nabla} \times \overleftrightarrow{G}^{(i)}(\boldsymbol{r},\boldsymbol{r}') \cdot \boldsymbol{J}\, dr'^2 = \frac{1}{4}\frac{\varepsilon_2-\varepsilon_1}{\varepsilon_2+\varepsilon_1}\boldsymbol{J}.} \tag{5.23}$$

5.2.1 Two Distinct Points on the Interface

We also need to take special care when $\boldsymbol{r}'$ and $\boldsymbol{r}$ are on the interface even though they are not coinciding. In this case $(z+z') \to 0$ and $\rho_r/(z+z') \to \infty$. Similarly to the previous section we have $\hat{\boldsymbol{n}} = -\hat{\boldsymbol{z}}$ and $\boldsymbol{J} = \hat{\boldsymbol{x}}J_x + \hat{\boldsymbol{y}}J_y$, therefore we can start this section with the following result

$$\overleftrightarrow{T} = -\frac{1}{4\pi}\frac{\varepsilon_2-\varepsilon_1}{\varepsilon_2+\varepsilon_1}\left\{ -\hat{\boldsymbol{\rho}}_{\boldsymbol{r}}\hat{\boldsymbol{\rho}}_{\boldsymbol{r}}\frac{z+z'}{\tilde{R}^3} + (\hat{\boldsymbol{\rho}}_{\boldsymbol{r}}\hat{\boldsymbol{\rho}}_{\boldsymbol{r}} - \hat{\boldsymbol{\varphi}}_{\boldsymbol{r}}\hat{\boldsymbol{\varphi}}_{\boldsymbol{r}})\frac{\tilde{R}-(z+z')}{\rho_r^2\tilde{R}}\right\}.$$

Now we can take the limit of the expression:

$$\lim_{(z+z')\to 0} \overleftrightarrow{T} = -\frac{1}{4\pi}\frac{\varepsilon_2-\varepsilon_1}{\varepsilon_2+\varepsilon_1}(\hat{\boldsymbol{\rho}}_{\boldsymbol{r}}\hat{\boldsymbol{\rho}}_{\boldsymbol{r}} - \hat{\boldsymbol{\varphi}}_{\boldsymbol{r}}\hat{\boldsymbol{\varphi}}_{\boldsymbol{r}})\frac{1}{\rho_r^2}, \tag{5.24}$$

we can see that if we integrate from $\varphi_r = 0$ to 2π there is no contribution, but if $(\rho_r, \varphi_r, 0)$ is not a point on the surface for a given φ_r, then this φ_r should not be integrated over, and there can be a net effect.

In the previous section we only considered a infinitesimal area ∂S, so it was enough to only consider the singular part of $\boldsymbol{\nabla}\times\overleftrightarrow{G}^{(i)}$. However, in this section we need to evaluate the integral over a finite area, and therefore we need to find the non singular part numerically. In effect what we need to do is replace $r^{(p)}(k_\rho)$ with $\left(r^{(p)}(k_\rho) - \frac{\varepsilon_2-\varepsilon_1}{\varepsilon_2+\varepsilon_1}\right)$, which goes to zero for large k_ρ, and add (5.24) to the evaluation. The integrand will be a slowly decreasing oscillating function, which will converge eventually, but it is not trivial to evaluate, we will see how to deal with that problem later.

5.2.2 Coinciding Points Above the Interface

In this case $\rho_r \to 0$ but $(z+z')/\rho_r \to \infty$, note that this case can also happen if $\boldsymbol{r}'$ and $\boldsymbol{r}$ is directly above or below one another, even if one of them is on the interface. The problems with this case is primarily that φ_r is undefined and secondarily that we need to find what happens to the Bessel functions when the argument is zero. The exponential will be decreasing for $k_\rho > k_1$, and the integral can be stopped for a relatively low k_ρ, so we must have $\lim_{\rho_r \to 0^+} k_\rho = 0$.

Recall the definition for the derivatives of the Bessel functions (5.19), and note that $\mathrm{J}_0(0) = 1$ and $\mathrm{J}_1(0) = 0$. Now we need to take the $\rho_r \to 0$ limit of all the terms in the curl of the indirect tensor, fortunately there are only three unique terms to evaluate

$$\lim_{\rho_r \to 0^+} \mathrm{J}_0'(k_\rho \rho_r) = 0,$$

$$\lim_{\rho_r \to 0^+} \frac{\mathrm{J}_0'(k_\rho \rho_r)}{k_\rho \rho_r} = \lim_{x \to 0^+} -\frac{\mathrm{J}_1(x)}{x} \overset{\text{L'Hôpital}}{=} \lim_{x \to 0^+} -\frac{1}{2}\left(\mathrm{J}_0(x) - \mathrm{J}_2(x)\right) = -\frac{1}{2},$$

$$\lim_{\rho_r \to 0^+} \mathrm{J}_0''(x) = \lim_{x \to 0^+} -\mathrm{J}_0(x) + \frac{1}{x}\mathrm{J}_1(x) = -\frac{1}{2},$$

in the second expression L'Hôpital's rule has been used and that $\mathrm{J}_m'(x) = \frac{1}{2}\left(\mathrm{J}_{m-1}(x) - \mathrm{J}_{m+1}(x)\right)$ and $\mathrm{J}_2(0) = 0$. These expressions can be put back into the tensor:

$$\boldsymbol{\nabla} \times \overleftrightarrow{G}^{(i)}(\boldsymbol{r}, \boldsymbol{r}') = \left(\hat{\boldsymbol{\varphi}}_{\boldsymbol{r}} \hat{\boldsymbol{\rho}}_{\boldsymbol{r}} - \hat{\boldsymbol{\rho}}_{\boldsymbol{r}} \hat{\boldsymbol{\varphi}}_{\boldsymbol{r}}\right) \frac{1}{8\pi} \int_0^\infty \left\{ r^{(p)}(k_\rho) - r^{(s)}(k_\rho) \right\} k_\rho e^{ik_{z,1}(z+z')}\, dk_\rho \quad (5.25)$$

The unit vectors are dependent on φ_r which is undefined, but they can be written in terms of Cartesian unit vectors instead:

$$\begin{aligned} \hat{\boldsymbol{\varphi}}_{\boldsymbol{r}} \hat{\boldsymbol{\rho}}_{\boldsymbol{r}} - \hat{\boldsymbol{\rho}}_{\boldsymbol{r}} \hat{\boldsymbol{\varphi}}_{\boldsymbol{r}} = &- \sin\varphi_r \cos\varphi_r \hat{\boldsymbol{x}}\hat{\boldsymbol{x}} - \sin^2\varphi_r \hat{\boldsymbol{x}}\hat{\boldsymbol{y}} + \cos^2\varphi_r \hat{\boldsymbol{y}}\hat{\boldsymbol{x}} + \cos\varphi_r \sin\varphi_r \hat{\boldsymbol{y}}\hat{\boldsymbol{y}} \\ &+ \sin\varphi_r \cos\varphi_r \hat{\boldsymbol{x}}\hat{\boldsymbol{x}} - \cos^2\varphi_r \hat{\boldsymbol{x}}\hat{\boldsymbol{y}} + \sin^2\varphi_r \hat{\boldsymbol{y}}\hat{\boldsymbol{x}} - \cos\varphi_r \sin\varphi_r \hat{\boldsymbol{y}}\hat{\boldsymbol{y}} \\ = &\ \hat{\boldsymbol{y}}\hat{\boldsymbol{x}} - \hat{\boldsymbol{x}}\hat{\boldsymbol{y}}, \end{aligned}$$

and the φ_r dependence is eliminated.

5.3 Integration of a Descending Oscillating Function

Way we have a function $f(x)$ that behaves as a slowly descending oscillating function for large arguments. Then the function's antiderivative $F(x)$ will converge to $F(\infty)$, but it will oscillate around this value and x may be very large before the oscillation amplitude is smaller than the acceptable error margin. Thus the challenge is to find $F(\infty)$ without integrating until a large upper bound.

If F behaves sinusoidally for large arguments and as the sine function crosses zero exactly at the point of largest rate of descent or ascent, then $F(\infty)$ can be found by evaluating F at one of these points. These points are simply the extrema of $f(x)$, thus we have $F(\infty) \approx F(x_n)$, where $f(x_n)$ is the $n'th$ extrema, for large n.

In Figure 5.3 this process has been applied to the $\mathrm{J}_0(x)$ function, it can be shown analytically that $\int_0^\infty \mathrm{J}_0(x)dx = 1$. We can see that the integral can be approximated well by stopping at extrema, but it is not perfect. Evaluating the antiderivative at minima tends to overestimate the convergence value and evaluating at maxima underestimates it, at least for J_0, this explains why the mean of the two is much better. As we can see the error for the mean solution quickly dives below 10^{-3}, thus we have found a way of estimating the improper integral of $f(x)$ as an average, which can be written as

$$\int_0^\infty f(x)dx \approx \int_0^{x_n} f(x)dx + \frac{1}{2}\int_{x_n}^{x_{n+1}} f(x)dx, \tag{5.26}$$

for sufficiently large n. Fortunately it seems that n can be small.

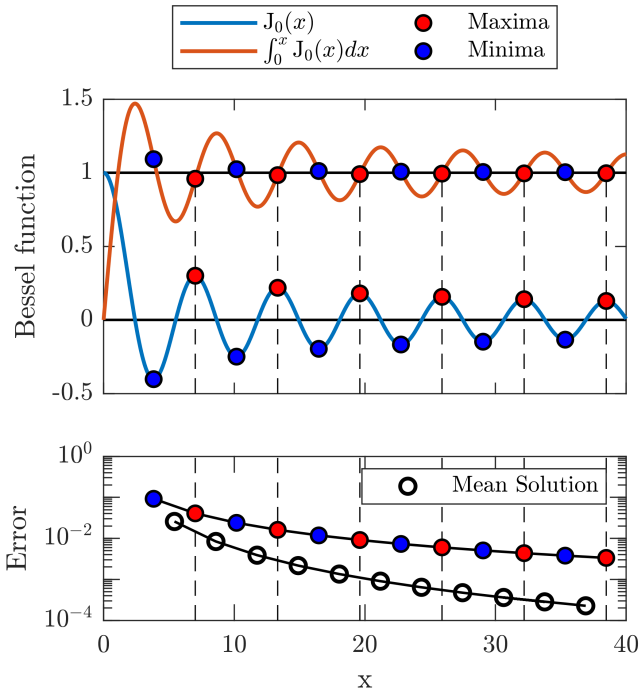

Figure 5.3: (Top picture) The Bessel function $\mathrm{J}_0(x)$ and its antiderivative, which oscillates around and converges to 1. The local maxima and minima of $J_0(x)$ corresponds to the highest rate of ascent and descent on the antiderivate, the value of the antiderivative at these points approaches 1. (Bottom picture) The absolute distance from 1 for the antiderivate evaluated at the maxima and minima points. The open circles represent the mean of the antiderivate for the two adjacent maxima and minima points, the mean solution approaches 1 much faster.

Chapter 6

Conclusion

Both the Facet Method and the Curvilinear Method as developed in this report gave accurate results compared to the analytical solution for the scattering caused by a PEC sphere. We saw that there are significant benefits of representing the scatterer surface exactly (CM) rather than as a faceted surface (FM). However the shape of the scatterer is somewhat limited in that it has to be made of spherical, cylindrical and flat segments. In the case of a sphere we saw that the sidelengths of the triangles must be much smaller than the incident wavelength, and decreasing the sidelengths is costly in terms of memory and time, so this is not a good model far wavelengths that are much smaller than the scatterer. For long wavelengths there is excellent agreement between the analytical and numerical result at least if the surface is exact and the integrals are approximated by subdivison rather than the centroidal approximation, interestingly the FM performs worse with subdivision.

The results for a rod are more mixed. The CM gives roughly the same results as another GFSIEM model that take advantage of cylindrical symmetry. The CM converges for some wavelengths, and the results here are probably close to what would actually happen, however for large wavelengths close to the global peak of the scattering cross section, the convergence is very slow. The fact that it happens for relatively large wavelengths is conflicting with the experience from the spherical case. The assumption that the current is constant over each triangle is probably the largest source for error, so the next step would be to have a linearly or quadratically varying current. Still the CM can be applied to wide variety of problems, with trustworthy results as long as it can converge without a prohibitively large number of triangles N.

The current is found on the basis of the MFIE, which has allowed us to analytically find the contribution from the singularity, and we have avoided any need for evaluating the integrals numerically. The model is expanded to also work for a scatterer in the presence of an interface in Chapter 5. If the scatterer is placed on the interface then this leads to a singular integrand, but this was also solved analytically.

Bibliography

[1] Walton C. Gibson. *The Method of Moments in Electromagnetics*. 1. ed. Chapman & Hall/CRC, 2008. ISBN: 978-1-4200-6145-1.

[2] David J. Griffiths. *Introduction to Electrodynamics*. 4. ed. Pearson Education, 2013. ISBN: 978-81-203-4776-2.

[3] Lukas Novotny and Bert Hecht. *Principles of Nano-Optics*. 2. ed. Cambridge University Press, 2012. ISBN: 978-1-107-00546-4.

[4] Thomas Garm Pedersen. *Electric, Optical & Magnetic Properties of Nanostructures*. Available at `http://homes.nano.aau.dk/tgp/` [accessed May 2020]. Aalborg University, 2019.

[5] Thomas M. Søndergaard. *Green's Function Integral Equation Methods in Nano-Optics*. 1. ed. CRC Press, 2019. ISBN: 978-0-8153-6596-9.

[6] Murray R. Spiegel and John Liu. *Mathematical Handbook of Formulas and Tables*. 2. ed. Schaum's Outlines. ISBN: 978-0070382039.

[7] Eric W. Weisstein. *Spherical Triangle*. MathWorld. URL: `https://mathworld.wolfram.com/SphericalTriangle.html` (visited on 05/08/2020).

[8] Eric W. Weisstein. *Spherical Trigonometry*. MathWorld. URL: `https://mathworld.wolfram.com/SphericalTrigonometry.html` (visited on 05/08/2020).

Appendix A

Analytic Solution for a Sphere

The scattering of plane waves hitting a homogeneous sphere, can be found analytically without making any assumptions with regard to the size of the sphere compared to the incident wavelength, this is the Mie solution. It is crucial to find a problem that can be solved analytically to compare with the numerical model and quantify how well the model works. In this chapter the results from [4, chapter 26] are used, although we will make some adaptions because we are interested in finding the surface current of a spherical perfect conductor. For a spherical particle it is convenient to use spherical coordinates where r is the radial distance, φ is the azimuthal angle and θ is the polar angle.

If the incident plane wave is x-polarized and traveling along the positive z-direction, $\boldsymbol{E} = \hat{\boldsymbol{x}}e^{ikz}$, then according to [4] the electric field can be written in terms of spherical waves as

$$E_0(\boldsymbol{r}) = \hat{\boldsymbol{x}}E_0e^{ikz} = E_0\sum_{n=1}^{\infty} i^n \frac{2n+1}{n(n+1)}\left\{\boldsymbol{M}_{o1n}^{(1)} - i\boldsymbol{N}_{e1n}^{(1)}\right\}, \tag{A.1}$$

where

$$M_{o1n}^{(1)} = \frac{\cos\varphi}{sin\theta}P_n^1(\cos\theta)j_n(kr)\hat{\boldsymbol{\theta}} - \sin\varphi\frac{\partial P_n^1(\cos\theta)}{\partial\theta}j_n(kr)\hat{\boldsymbol{\varphi}},$$

$$N_{e1n}^{(1)} = \cos\varphi P_n^1(\cos\varphi)n(n+1)\frac{j_n(kr)}{kr}\hat{\boldsymbol{r}} + \frac{[krj_n(kr)]'}{kr}\left[\cos\varphi\frac{\partial P_n^1(\cos\theta)}{\partial\theta}\hat{\boldsymbol{\theta}} - \sin\varphi\frac{P_n^1(\cos\theta)}{\sin\theta}\hat{\boldsymbol{\varphi}}\right],$$

where $P_n^1(\cos\theta)$ is an associated Legendre polynomial, using the positive sign convention: $P_n^1(x) = \sqrt{1-x^2}\frac{dP_n(x)}{dx}$, $j_n(kr)$ is the spherical Bessel function given by

$$j_n(kr) = \sqrt{\frac{\pi}{2kr}}\,\mathrm{J}_{n+1/2}(kr),$$

and

$$[krj_n(kr)]' = \left.\frac{\partial[kr'j_n(kr')]}{\partial kr'}\right|_{r'=r} = \frac{1}{2}\sqrt{\frac{\pi}{2}}\left[\frac{\mathrm{J}_{n+1/2}(kr)}{\sqrt{kr}} + \sqrt{kr}\left(\mathrm{J}_{n-1/2}(kr) - \mathrm{J}_{n+3/2}(kr)\right)\right].$$

The scattered electric field is given by

$$E_{\text{scat}}(\boldsymbol{r}) = \sum_{n=1}^{\infty} i^n \frac{2n+1}{n(n+1)} \left\{ a_n \boldsymbol{M}_{o1n}^{(2)} - i b_n \boldsymbol{N}_{e1n}^{(2)}, \right\} \tag{A.2}$$

where the superscript (2) of $\boldsymbol{M}$ and $\boldsymbol{N}$ denotes that the spherical Bessel function is exchanged with a spherical Hankel function $h_n(kr) = \mathrm{J}_{n+1/2}(kr) + i\mathrm{Y}_{n+1/2}(kr)$, where $Y_n(x)$ is the Bessel function of second kind. The coefficients a_n and b_n can be found by enforcing our boundary condition: $\hat{\boldsymbol{n}} \times \boldsymbol{E} = 0$ at $r = a$. thus the tangential part of the field must be zero $(\boldsymbol{E}_0(r = a, \theta, \varphi) + \boldsymbol{E}_{\text{scat}}(r = a, \theta, \varphi)) \cdot \hat{\boldsymbol{\varphi}} = 0$, now the coefficients can be found

$$a_n = -\frac{j_n(ka)}{h_n(ka))'}, \qquad b_n = -\frac{[kaj_n(ka)]'}{[kah_n(ka)]'}. \tag{A.3}$$

The corresponding incoming and scattered magnetic field can be found by using $\boldsymbol{H}(\boldsymbol{r}) = \frac{-i}{\omega\mu_0} \boldsymbol{\nabla} \times \boldsymbol{E}(\boldsymbol{r})$ and that $\nabla \times \boldsymbol{M} = k\boldsymbol{N}$ and $\nabla \times \boldsymbol{N} = k\boldsymbol{M}$:

$$\boldsymbol{H}_0 = -i\sqrt{\frac{\varepsilon_0}{\mu_0}} n_1 E_0 \sum_{n=1}^{\infty} i^n \frac{2n+1}{n(n+1)} \left\{ \boldsymbol{N}_{o1n}^{(1)} - i\boldsymbol{M}_{e1n}^{(1)} \right\} \tag{A.4}$$

$$\boldsymbol{H}_{\text{scat}} = -i\sqrt{\frac{\varepsilon_0}{\mu_0}} n_1 E_0 \sum_{n=1}^{\infty} i^n \frac{2n+1}{n(n+1)} \left\{ a_n \boldsymbol{N}_{o1n}^{(2)} - i b_n \boldsymbol{M}_{e1n}^{(2)} \right\} \tag{A.5}$$

where

$$\boldsymbol{M}_{e1n}^{(1)} = \frac{-\sin\varphi}{sin\theta} P_n^1(\cos\theta) j_n(kr) \hat{\boldsymbol{\theta}} - \cos\varphi \frac{\partial P_n^1(\cos\theta)}{\partial\theta} j_n(kr) \hat{\boldsymbol{\varphi}},$$

$$\boldsymbol{N}_{o1n}^{(1)} = \sin\varphi P_n^1(\cos\varphi) n(n+1) \frac{j_n(kr)}{kr} \hat{\boldsymbol{r}} + \frac{[krj_n(kr)]'}{kr} \left[\sin\varphi \frac{\partial P_n^1(\cos\theta)}{\partial\theta} \hat{\boldsymbol{\theta}} + \cos\varphi \frac{P_n^1(\cos\theta)}{\sin\theta} \hat{\boldsymbol{\varphi}} \right].$$

We are interested in the current, $\boldsymbol{J} = \hat{\boldsymbol{n}} \times \boldsymbol{H}$, with spherical symmetry the normal vector is given by $\hat{\boldsymbol{n}} = \hat{\boldsymbol{r}}$, which means that $\hat{\boldsymbol{n}} \times \hat{\boldsymbol{\varphi}} = -\hat{\boldsymbol{\theta}}$, and $\hat{\boldsymbol{n}} \times \hat{\boldsymbol{\theta}} = \hat{\boldsymbol{\varphi}}$, thus the $\hat{\boldsymbol{\theta}}$ and $\hat{\boldsymbol{\varphi}}$-component of the surface current is

$$J_\varphi(\theta, \varphi) = -i\sqrt{\frac{\varepsilon_0}{\mu_0}} n_1 E_0 \sum_{n=1}^{\infty} i^n \frac{2n+1}{n(n+1)} \left\{ \frac{sin\varphi}{ka} \frac{\partial P_n^1(\cos\theta)}{\partial\theta} \left[[kaj_n(ka)]' + a_n [kah_n(ka)]' \right] \right.$$
$$\left. + i\frac{\sin\varphi}{\sin\theta} P_n^1(\cos\theta) [j_n(ka) + b_n h_n(ka)] \right\} \tag{A.6}$$

$$J_\theta(\theta, \varphi) = +i\sqrt{\frac{\varepsilon_0}{\mu_0}} n_1 E_0 \sum_{n=1}^{\infty} i^n \frac{2n+1}{n(n+1)} \left\{ \frac{\cos\varphi}{ka} \frac{P_n^1(\cos\theta)}{\sin\theta} \left[[kaj_n(ka)]' + a_n [kah_n(ka)]' \right] \right.$$
$$\left. + i\cos\theta \frac{\partial P_n^1(\cos\theta)}{\partial\theta} [j_n(ka) + b_n h_n(ka)] \right\} \tag{A.7}$$

A.1 Scattering Cross Section

Both the differential and integral scattering cross section can be found analytically as well.

The differential cross section is given by

$$\frac{\partial \sigma_{sc}(\theta, \varphi)}{\partial \Omega} = \gamma_p(\theta) \cos^2 \varphi + \gamma_s(\theta) \sin^2 \varphi, \tag{A.8}$$

where γ_p is the differential scattering cross section in the xz-plane and γ_s is in the yz-plane, and they are given by

$$\gamma_p(\theta) = \frac{1}{k^2} \left| \sum_{n=1}^{\infty} \frac{2n+1}{n(n+1)} \left(a_n \frac{P_n^1(\cos\theta)}{\sin\theta} + b_n \frac{\partial P_n^1(\cos\theta)}{\partial \theta} \right) \right|^2, \tag{A.9}$$

$$\gamma_s(\theta) = \frac{1}{k^2} \left| \sum_{n=1}^{\infty} \frac{2n+1}{n(n+1)} \left(a_n \frac{\partial P_n^1(\cos\theta)}{\partial \theta} + b_n \frac{P_n^1(\cos\theta)}{\sin\theta} \right) \right|^2. \tag{A.10}$$

The scattering cross section can be found by integrating the differential cross section over the full solid angle $\sigma = \oint_{4\pi} \frac{\partial \sigma(\theta,\varphi)}{\partial \Omega} \, d\Omega$, which turns out to be

$$\sigma_{sc} = \frac{2\pi}{k^2} \sum_{n=1}^{\infty} (2n+1) \left\{ |a_n|^2 + |b_n|^2 \right\}. \tag{A.11}$$

The differential and integral scattering cross section is illustrated in Figure A.1 below.

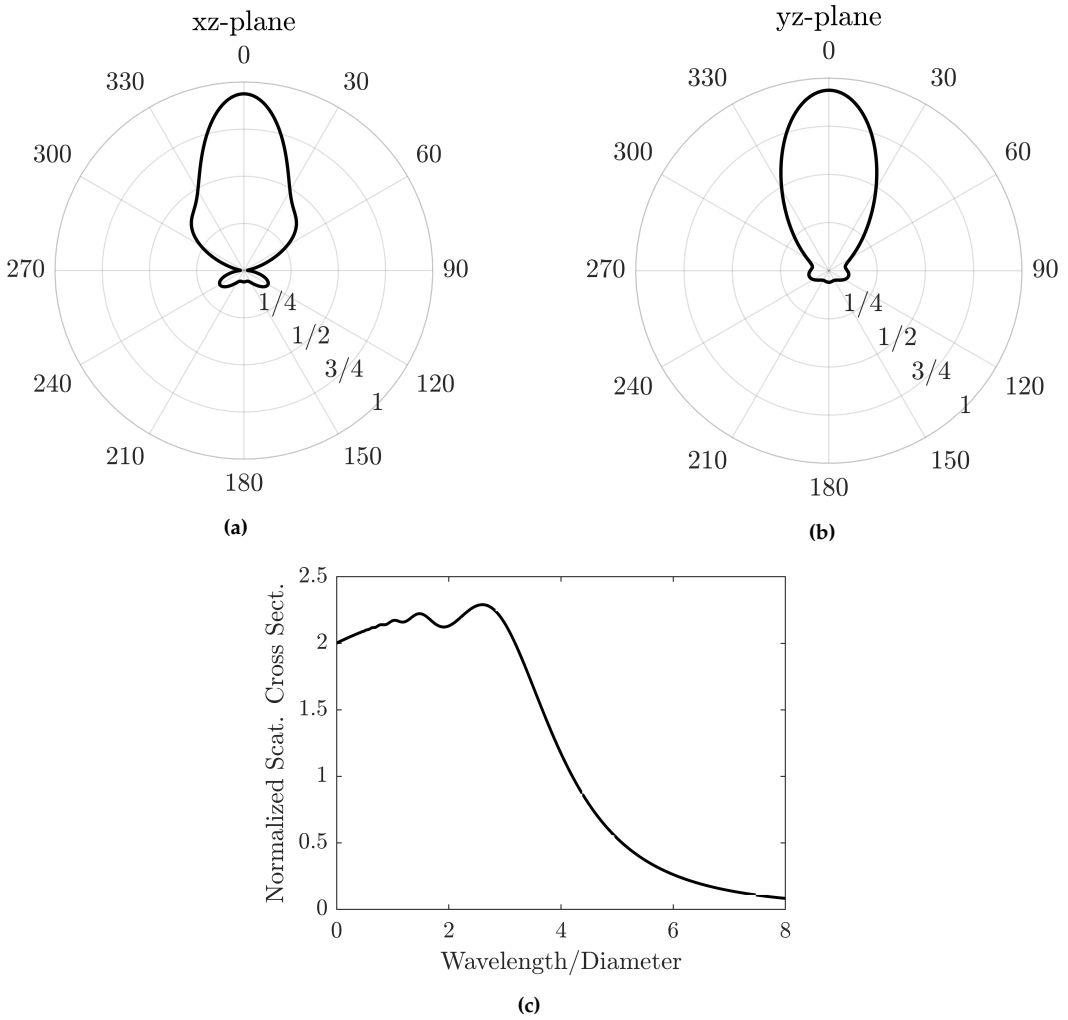

Figure A.1: Differential and total scattering cross section for a PEC ball illuminated by a x-polarized plane wave traveling along the positive z-axis. The cross sections are normalized with regard to the geometrical cross section of the ball, πa^2. **(a)** Shows the differential cross section in the xz-plane, where the incident field has a wavelength equal to the diameter of the ball, **(b)** is the same for the yz-plane. **(c)** is the total scattering cross section, which goes to 2 for small wavelengths and to 0 for large wavelengths.